Arf-like GTPase Arl8b regulates lytic granule polarization and natural killer cell–mediated cytotoxicity

Amit Tuli[a,b], Jerome Thiery[c,d], Ashley M. James[e], Xavier Michelet[a], Mahak Sharma[a,f], Salil Garg[a], Keri B. Sanborn[c,e], Jordan S. Orange[e,g], Judy Lieberman[c], and Michael B. Brenner[a]

[a]Division of Rheumatology, Immunology and Allergy, Department of Medicine, Brigham and Women's Hospital, Harvard Medical School, Boston, MA 02115; [b]Division of Cell Biology and Immunology, Institute of Microbial Technology, Chandigarh 160036, India; [c]Program in Cellular and Molecular Medicine, Boston Children's Hospital, Harvard Medical School, Boston, MA 02115; [d]Institut National de la Santé et de la Recherche Médicale, Unité 753, Institut Gustave Roussy, Villejuif 75654, France; [e]Department of Pediatrics, University of Pennsylvania School of Medicine, Philadelphia, PA 19104; [f]Department of Biological Sciences, Indian Institute of Science Education and Research, Mohali 140306, India; [g]Immunology, Allergy and Rheumatology, Texas Children's Hospital, Baylor College of Medicine, Houston, TX 77030

ABSTRACT **Natural killer (NK) lymphocytes contain lysosome-related organelles (LROs), known as lytic granules, which upon formation of immune synapse with the target cell, polarize toward the immune synapse to deliver their contents to the target cell membrane. Here, we identify a small GTP-binding protein, ADP-ribosylation factor-like 8b (Arl8b), as a critical factor required for NK cell–mediated cytotoxicity. Our findings indicate that Arl8b drives the polarization of lytic granules and microtubule-organizing centers (MTOCs) toward the immune synapse between effector NK lymphocytes and target cells. Using a glutathione *S*-transferase pull-down approach, we identify kinesin family member 5B (KIF5B; the heavy chain of kinesin-1) as an interaction partner of Arl8b from NK cell lysates. Previous studies showed that interaction between kinesin-1 and Arl8b is mediated by SifA and kinesin-interacting protein (SKIP) and the tripartite complex drives the anterograde movement of lysosomes. Silencing of both KIF5B and SKIP in NK cells, similar to Arl8b, led to failure of MTOC-lytic granule polarization to the immune synapse, suggesting that Arl8b and kinesin-1 together control this critical step in NK cell cytotoxicity.**

Monitoring Editor
Thomas F. J. Martin
University of Wisconsin

Received: May 16, 2013
Revised: Sep 11, 2013
Accepted: Sep 25, 2013

INTRODUCTION

Lysosome-related organelles (LROs) are specialized compartments that store secretory cargo for regulated exocytosis in response to external stimuli (Dell'Angelica *et al.*, 2000; Stinchcombe and Griffiths, 2007). Examples of LROs include melanosomes, lytic granules in cytotoxic T lymphocytes (CTLs) and natural killer (NK) cells, basophil granules, platelet-dense granules, neutrophil azurophilic granules, and dense-core vesicles in endocrine cells (Burkhardt *et al.*, 1990; Bonifacino, 2004; Raposo and Marks, 2007). LROs, like conventional lysosomes, contain vacuolar ATPases to maintain a low pH, acid hydrolases, and common membrane-associated proteins, such as LAMP-1 (CD107a), LAMP-2 (CD107b), and CD63 (Bonifacino, 2004; Benado *et al.*, 2009).

Lysosomes and LROs are dynamic organelles that associate with molecular motors to traffic along the cytoskeleton (Hirokawa, 1998). Microtubule- and actin-based motility plays a critical role in controlling the function of lysosomes and LROs. For example, during nutrient starvation, lysosomal association with kinesin motor proteins is reduced, which disrupts the normal peripheral distribution of lysosomes (Korolchuk *et al.*, 2011). This decreases the interaction between upstream signaling modules localized near the plasma

This article was published online ahead of print in MBoC in Press (http://www.molbiolcell.org/cgi/doi/10.1091/mbc.E13-05-0259) on October 2, 2013.

Address correspondence to: Amit Tuli (atuli@imtech.res.in), Michael B. Brenner (mbrenner@research.bwh.harvard.edu).

Abbreviations used: Arl8a, ADP-ribosylation factor-like 8a; Arl8b, ADP-ribosylation factor-like 8b; CTL, cytotoxic T-lymphocyte; EEA1, early endosome antigen 1; EM, electron microscopy; GzmB, granzyme B; GST, glutathione *S*-transferase; KHC, kinesin heavy chain; KIF5B, kinesin family member 5B; LRO, lysosome-related organelle; MTOC, microtubule-organizing center; mTOR, mammalian target of rapamycin; NK, natural killer; PBS, phosphate-buffered saline; PFA, paraformaldehyde; Pfn, perforin; qRT-PCR, quantitative reverse transcriptase PCR; Rab27a, Ras-related protein Rab-27a; shRNA, short hairpin RNA; siRNA, small interfering RNA; SKIP, SifA and kinesin-interacting protein.

Supplemental Material can be found at:
http://www.molbiolcell.org/content/suppl/2013/09/30/mbc.E13-05-0259.DC1.html

membrane and the lysosome-associated mammalian target of rapamycin (mTOR) complex, preventing the activation of mTOR, which is required for new protein synthesis. Simultaneously, starvation-induced autophagosome fusion with lysosomes increases with perinuclear clustering of lysosomes as both organelles group near the microtubule-organizing center (MTOC). Degradation of autophagic contents in the lysosomes then releases necessary nutrients for cell survival during starvation. Lysosomal motility not only is important for cellular homeostasis, but also is altered in certain pathological states (Kirkegaard and Jaattela, 2009). For example, in some tumor cells, lysosomes move toward the cell periphery and fuse with the plasma membrane to release lysosomal proteases that degrade the extracellular matrix to promote tumor invasion and metastasis (Mohamed and Sloane, 2006).

For some LROs, motility control is even more critical since these secretory organelles need to move rapidly to fuse with the plasma membrane to release their contents after receiving external stimuli. When an immunological synapse forms between killer cells and a target cell destined for immune elimination, lytic granules are mobilized toward the MTOC via microtubule minus end–directed dynein/dynactin motor proteins. Then the lytic granules polarize toward and then fuse with the plasma membrane to release their lytic contents into the synapse adjacent to the target cell membrane (Stinchcombe and Griffiths, 2007; Orange, 2008). Some LROs are transferred from microtubules to myosin motors associated with the cortical actin network just beneath the plasma membrane to enable vesicle docking and subsequent fusion with the cell membrane (Fukuda *et al.*, 2002).

For motility to occur, motor proteins are recruited to bind to small GTP-binding proteins of the Rab family located on the outer surface of organelle membranes (Horgan and McCaffrey, 2011). Rab6 and Rab14 directly bind kinesin motor proteins KIF20A and KIF16B, respectively, to deliver cargo to and from the Golgi (Echard *et al.*, 1998; Hill *et al.*, 2000; Ueno *et al.*, 2011). Often, GTP-bound Rab proteins recruit a linker protein (Rab effector) that couples a Rab protein with its cognate motor protein. For example, RILP couples Rab7 on late endosomes to the p150 subunit of dynein/dynactin to control the inward motility of late endosomes toward the MTOC (Jordens *et al.*, 2001). Ras-related protein Rab-27a (Rab27), a Rab protein used by several LROs, binds in melanosomes to a melanocyte-specific effector protein, melanophilin, that links it to the actin-based motor, myosin Va, to mediate melanosome transfer from microtubules to the actin network (Fukuda *et al.*, 2002; Strom *et al.*, 2002; Wu *et al.*, 2002). This step is critical for melanosome transfer to neighboring keratinocytes for skin pigmentation (Hume and Seabra, 2011). Of interest, loss-of-function mutation in one of several proteins (Rab27a, melanophilin, or myosin Va) leads to Griscelli syndrome, an autosomal recessive disorder associated with hypopigmentation (Mercer *et al.*, 1991; Menasche *et al.*, 2000; Matesic *et al.*, 2001). Mutations in Rab27 and a different myosin (myosin IIa) also lead to a loss of cytotoxicity by killer lymphocytes (Haddad *et al.*, 2001; Stinchcombe *et al.*, 2001; Fukuda, 2006; Liu *et al.*, 2010).

A ubiquitously expressed member of the Arf-like family of small G proteins, ADP-ribosylation factor-like 8b (Arl8b), was shown to be required for endocytic trafficking toward conventional lysosomes, as well as for lysosomal spatial distribution in the cell (Hofmann and Munro, 2006; Donaldson and Jackson, 2011; Garg *et al.*, 2011). Arl8b controls the spatial distribution of lysosomes by regulating their motility on microtubule tracks (Bagshaw *et al.*, 2006; Hofmann and Munro, 2006). Overexpression of Arl8b drives lysosomes toward the cell periphery, whereas Arl8b silencing causes clustering of lysosomes at the MTOC. Arl8b associates with the plus-end motor kinesin-1 (also known as kinesin family member 5B [KIF5B]) via a linker protein, SifA and kinesin-interacting protein (SKIP), and the tripartite complex drives lysosomes to the cell periphery (Rosa-Ferreira and Munro, 2011). It is not known whether Arl8b associates with LROs and has a role in their trafficking.

Here we show that Arl8b is localized to lytic granules in NK cells and is required for NK cell–mediated cytotoxicity. Arl8b drives movement of lytic granules toward the immune synapse formed between NK lymphocytes and their target cells. MTOC polarization toward the immune synapse also requires Arl8b. KIF5B (the heavy chain of kinesin-1) is the interaction partner of Arl8b. Silencing of either KIF5B or Arl8b, as well as of their interaction partner SKIP, in NK cells leads to a failure of MTOC–lytic granule polarization to the immune synapse, suggesting that Arl8b and kinesin-1 together control this critical step in NK cell cytotoxicity.

RESULTS

Arl8b localizes to lytic granules of NK cells

Several studies implicate Arl8b in controlling the microtubule-based motility of conventional lysosomes (Bagshaw *et al.*, 2006; Hofmann and Munro, 2006; Rosa-Ferreira and Munro, 2011). Given that LROs share certain features with lysosomes, we explored whether Arl8b regulates the motility and exocytosis of LROs. To answer this question, we first examined the localization of endogenous Arl8b to determine whether Arl8b associates with LROs in the YT-Indy human NK cell line (Yodoi *et al.*, 1985; Wagtmann *et al.*, 1995). Arl8b colocalized with perforin (Pfn), granzyme B (GzmB) markers for lytic granules, and LAMP-1, a marker for both lysosomes and lytic granules, but not with the early endosomal marker early endosome antigen 1 (EEA1; Figure 1, A–D, and Supplemental Figure S1). Colocalization with all these various proteins was quantified and clearly indicates association of Arl8b with lytic granules (Figure 1E). To biochemically confirm the presence of Arl8b on lytic granules, we probed YT-Indy cell lysate fractions, separated by density centrifugation to isolate organelles, for Arl8b, GzmB, and LAMP-1. Although their migration patterns were not identical, all three proteins were enriched in fractions 4–6 relative to the postnuclear lysate (Figure 1F). Actin was excluded from these fractions, confirming that the Arl8b-, LAMP-1–, and GzmB-containing fractions are enriched for granules. As a further confirmation of Arl8b presence on the surface of lytic granules, peptides corresponding to Arl8b were identified in a preparation from surface-biotinylated NK cell lytic granules using mass spectrometry (unpublished data). Published proteomic analyses also suggest that Arl8b is associated with a variety of LROs, including NK cell lytic granules, melanosomes, and neuromelanin granules (Casey *et al.*, 2007; Hu *et al.*, 2007).

Arl8b is required for lytic granule exocytosis by human NK cells

To address the function of Arl8b in NK cell lytic granules, we transduced YT-Indy NK cells with two unique short hairpin RNA (shRNA) sequences designed to specifically target Arl8b (Arl8b-407 and Arl8b-921) but not its homologue ADP-ribosylation factor-like 8a (Arl8a). The efficiency of gene knockdown was assessed by Western blotting and quantitative reverse transcriptase-PCR (qRT-PCR) using Arl8b-specific primers (Figure 2, A and B). Both Arl8b shRNAs reduced Arl8b protein expression by ~80–85% or more in YT-Indy cells compared with wild-type or control shRNA–transduced cells (Figure 2A, top). The Arl8b antiserum identified the protein as a doublet by Western blot, of which only the dominant lower band (~21 kDa) was

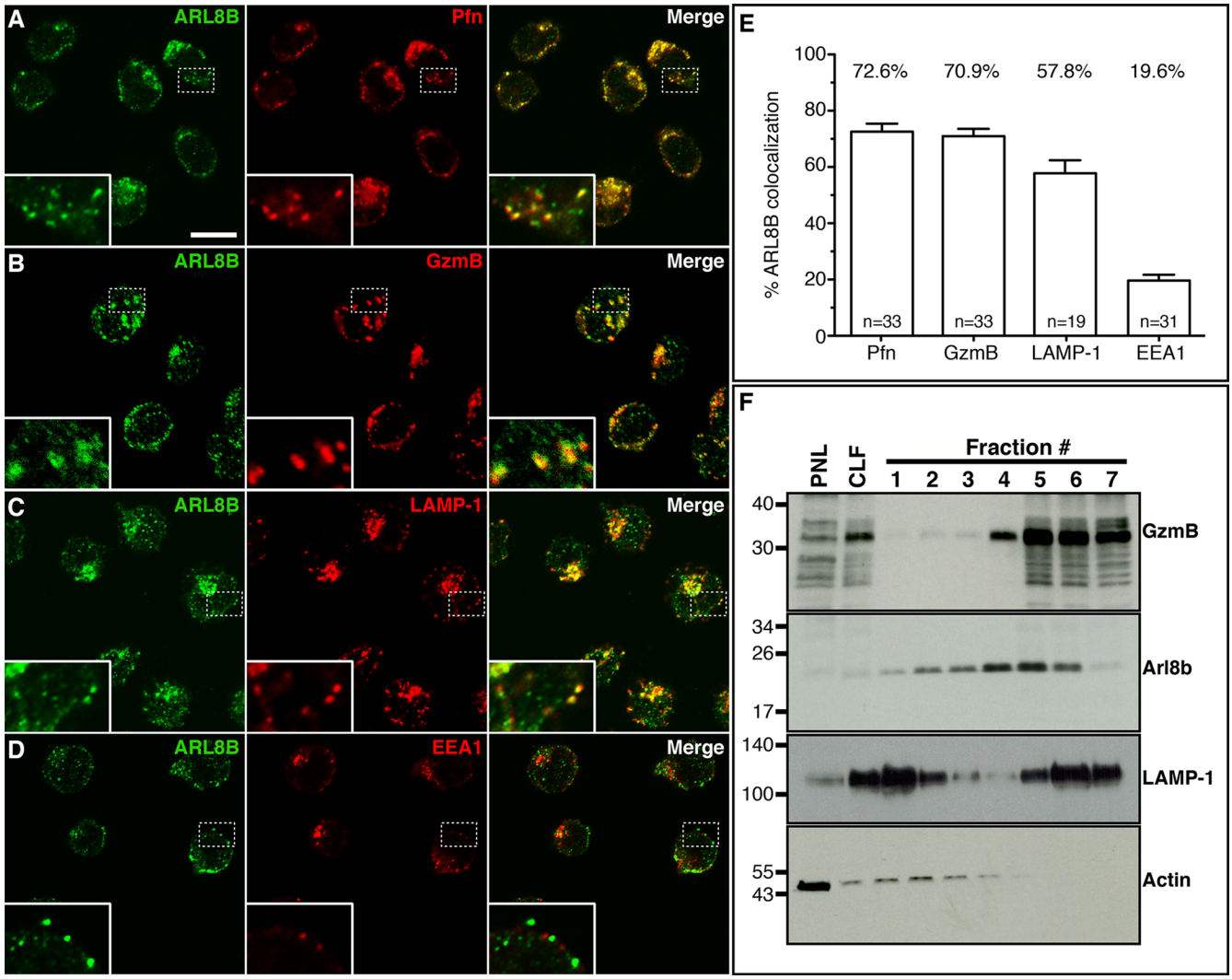

FIGURE 1: Arl8b localizes to lytic granules in NK cells. (A–D) Arl8b colocalizes with perforin, granzyme B, and LAMP-1, markers of lytic granules. YT-Indy cells were fixed and stained with anti-Arl8 (green), anti-perforin (red, A), anti-granzyme B (red, B), anti-LAMP-1 (red, C), and anti-EEA1 (red, D) antibodies, and analyzed by confocal microscopy. As shown in the inset, Arl8b strongly colocalizes with perforin, granzyme B, and LAMP-1 but not with EEA1 (marker for early endosomes). Scale bar, 10 μm. (E) Quantification of Arl8b-positive structures, showing colocalization with markers of lytic granules in YT-Indy cells. The graph displays the percentage of Arl8b colocalizing with perforin, granzyme B, LAMP-1, and EEA1. The values were obtained from the analysis of the following numbers of cells: Pfn, $n = 33$; GzmB, $n = 33$; LAMP-1, $n = 19$; and EEA1, $n = 31$. Error bars, SD. (F) Arl8b associates with lytic granules. Lytic granules were isolated from YT-Indy cells by density gradient separation and collected in seven equal-volume fractions (from least to most dense). Arl8b was identified in the lytic granule preparation by Western blot (second from top) and comigrated with granzyme B (top) and LAMP-1 (third from top). PNL and CLF, postnuclear lysate and crude lysosomal fraction, respectively, generated in preparing the starting material for the density gradient. The fractions were also probed for actin to demonstrate the general lack of cellular contamination during lytic granules isolation (bottom).

reduced by the Arl8b shRNA. The upper band was identified as Arl8a, which is 91% identical to Arl8b and shares the C-terminal peptide region used for generating the Arl8b antibody (Garg *et al.*, 2011). Arl8b-specific knockdown was confirmed by the qRT-PCR analysis, which showed an ~75–80% reduction in Arl8b mRNA but no significant change in Arl8a expression (Figure 2B). Arl8b knockdown did not change the levels of lytic proteins (perforin and granzyme B) in YT-Indy cells, as assessed by Western blot and flow cytometry (Figure 2A, middle, and unpublished data).

To test the effect of Arl8b silencing on NK cell cytotoxicity, we incubated YT-Indy cells stably transduced with control or Arl8b-specific shRNAs with 721.221 B-lymphoblastoid target cells and measured the percentage specific killing by ^{51}Cr-release assay. Arl8b silencing dramatically reduced NK cell cytotoxicity at all effector:target (E:T) ratios compared with the control shRNA treatment (Figure 2C). The reduction in cytotoxicity was somewhat greater in YT-Indy cells transduced with Arl8b 407shRNA compared with Arl8b 921shRNA, corresponding to the greater efficiency of the former shRNA in silencing Arl8b expression. To appreciate the importance of Arl8b function in mediating NK cell cytotoxicity, we compared the effect of Arl8b and Rab27a silencing (Figure 2E and Supplemental Figure S2B). Silencing of either GTPase in NK cells reduced target cell lysis comparably. Thus Arl8b is an important regulator of cytolytic killing by NK cells.

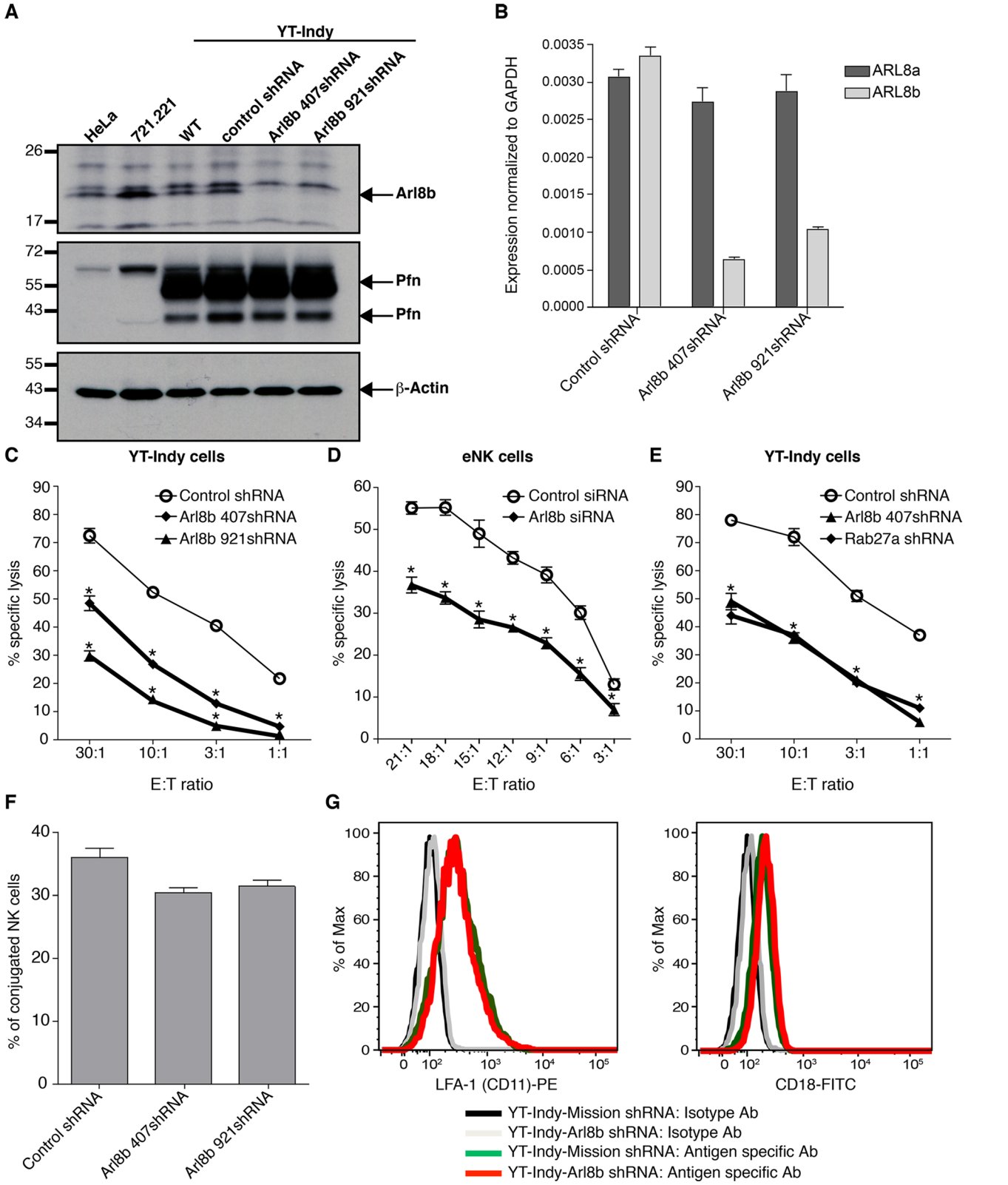

FIGURE 2: Arl8b regulates NK cell cytotoxicity. (A) Stable silencing of Arl8b expression in NK cells using two distinct shRNA sequences (407 and 921). Left, Western blot analyses of Arl8b (top), perforin (middle), and actin (bottom) levels in YT-Indy (untreated) and YT-Indy stably expressing lentiviral vector–driven control shRNA, Arl8b 407 shRNA, or Arl8b 921 shRNA, as indicated. HeLa and 721.221 cell lysates were used as a negative control for perforin, and actin was used as a protein loading control. (B) qRT-PCR analyses of Arl8b and Arl8a levels in control shRNA–, Arl8b 407shRNA–, and Arl8b 921shRNAxexpressing YT-Indy cells. (C–E) Down-regulation of Arl8b impairs NK cytotoxicity. Cytotoxicity of YT-Indy cells stably expressing control shRNA– or Arl8b-specific shRNA-407 and -921 (C), control- or Arl8b siRNA–treated (72 h) primary human NK cells (D), and YT-Indy cells stable expressing control shRNA, Arl8b-specific shRNA, or

The effect of Arl8b silencing on NK cell cytotoxicity was further confirmed using isolated human NK cells. Primary human NK cells were transfected with Arl8b-407siRNA instead of using lentiviral vector-driven shRNA, since lentiviral transduction was only effective after 7 d, when primary NK cell viability was already reduced. The small interfering RNA (siRNA) silenced Arl8b mRNA by >70% after 72 h by qRT-PCR (Supplemental Figure S2A). Silencing of Arl8b in primary NK cells also significantly reduced target cell lysis (Figure 2D).

The Arl8 family contains two members, Arl8a and Arl8b, that both localize to lysosomes (Hofmann and Munro, 2006). To evaluate the potential contribution of Arl8a in NK cell cytotoxicity, we compared the cytotoxic response in NK cells lacking Arl8a versus Arl8b. To stably silence Arl8a expression, YT-Indy cells were transduced with control or Arl8a-specific shRNAs (Arl8a 497shRNA and Arl8a 1685shRNA). Treatment of YT-Indy cells with Arl8a-specific shRNAs significantly reduced Arl8a expression (>80%) without altering Arl8b expression, as verified by quantitative RT-PCR (Supplemental Figure S3A). NK cells with reduced Arl8a also were less cytotoxic than control shRNA–treated cells; however, the loss in cytotoxicity was weaker than in NK cells in which Arl8b was silenced (Supplemental Figure S3B). These results suggest that Arl8b is the major isoform of the Arl8 family that regulates the function of both lysosomes and lytic granules. Because silencing both Arl8a and Arl8b severely reduced NK cell viability (knockdown of individual proteins had no significant effect on cell viability compared with control shRNA treatment; unpublished data), the effect of dual silencing on cytolytic activity could not be measured, suggesting a role of Arl8 isoforms in regulating other cellular vital functions besides NK cell cytotoxicity.

Arl8b does not affect NK cell–target conjugation

Formation of effector–target conjugates is a prerequisite for target cell lysis during NK cell cytotoxicity. To determine whether the reduced killing of target cells by NK cells with Arl8b silenced might be due to impaired conjugate formation, we prelabeled YT-Indy cells (control or Arl8b shRNA transduced) and 721.221 target cells with PKH26 (red) or PKH67 (green) cell membrane-labeling dyes, respectively, and coincubated them to enable formation of heterotypic cytolytic conjugates. Flow cytometry analysis of effector–target conjugates showed only a modest change in the percentage of conjugates formed by control or Arl8b-silenced cells, suggesting that Arl8b is not important in conjugate formation (Figure 2F). Silencing Arl8b in YT-Indy cells also did not affect the cell surface levels of the CD11a and CD18 subunits of the integrin lymphocyte function–associated antigen-1 (LFA-1; Figure 2G), which is critical for conjugate formation (Kohl *et al.*, 1984). Rapid actin cytoskeletal rearrangements are vital components of immune synapse formation and critical for stability of conjugates, as well as for many downstream cytolytic events (Orange *et al.*, 2003). To examine the effect of Arl8b silencing on F-actin polymerization at the immune synapse, we coincubated NK cells with anti-LFA-1–coated polystyrene beads to cross-link LFA-1 on the surface of NK cells and induce actin accumulation at the cell–bead interface (Chen *et al.*, 2007). There was no apparent difference in actin polymerization at the bead–cell contact area in YT-Indy cells transduced with control or Arl8b shRNA (Supplemental Figure S4A). Thus Arl8b is not required for the initial steps of effector–target conjugate formation.

Arl8b regulates polarization of lytic granules to the immune synapse

Arl8b plays a critical function in controlling microtubule-based motility of conventional lysosomes toward the cell periphery (Bagshaw *et al.*, 2006; Hofmann and Munro, 2006; Rosa-Ferreira and Munro, 2011). Because Arl8b also associates with lytic granules and lytic granule polarization at the immune synapse depends on microtubule-based movement, we hypothesized that Arl8b also regulates the motility of lytic granules toward the immune synapse. To test this hypothesis, we analyzed polarization of perforin-containing lytic granules toward the immune synapse of control or Arl8b-silenced YT-Indy cells, stably expressing CD2-GFP, during conjugation with 721.221 target cells. CD2 concentration at the immune synapse identifies activated NK cells in conjugates (Orange *et al.*, 2003). Both control and Arl8b shRNA–transduced YT-Indy cells formed similar numbers of conjugates that showed CD2 capping at the synapse (Figures 3, A–C). However, Arl8b silencing resulted in a dramatic decrease in lytic granule polarization to the immune synapse, indicated by the location of perforin-containing lytic granules (stained red) away from, rather than at, the immunological synapse (Figure 3, compare A with B and C). To quantify this effect, we analyzed lytic granule localization in >100 conjugates in three independent experiments of YT-Indy (control and Arl8b shRNA transduced) and 721.221 target cells stained with perforin antibody to mark lytic granules. The quantification was done by first identifying the conjugates in differential interference contrast images as cases in which substantial contact between the NK cell and the target cell occurred, and 100–150 conjugates were counted per condition per experiment. Conjugates were scored positive for polarization if the granules (based on perforin staining) were against the cell–cell interface. After 20 min of NK cell incubation with targets, 75 ± 4% of conjugates formed by control shRNA–transduced cells showed complete granule polarization toward the immune synapse, whereas only 30 ± 5 and 37 ± 6% of conjugates formed by Arl8b 407shRNA– and Arl8b 921shRNA–transduced YT-Indy cells, respectively, had polarized granules (Figure 3D). A similar analyses performed on conjugates of NK cells transduced with Arl8a shRNA showed no significant difference in granule polarization compared with the control conjugates, indicating that the lack of Arl8b, but not of Arl8a, results in loss of lytic granule polarization (Supplemental Figure S4B). These results support our previous unpublished observations that depletion of Arl8a does not induce clustering of lysosomes in other cell types.

Rab27a-specific shRNA (E) was tested against 721.221 target cells by ^{51}Cr-release assay at various E:T ratios. Data show mean ± SEM from triplicates of one representative experiment of three performed; $*p < 0.05$. (F) Silencing of Arl8b does not affect conjugate formation. YT-Indy cells (control or Arl8b shRNA transduced) and 721.221 target cells were stained with PKH26 (Red Fluorescent Cell Linker) and PKH67 (Green Fluorescent Cell Linker), respectively. Labeled cells were coincubated at a 2:1 E:T ratio for 20 min, fixed in 4% PFA, and analyzed by flow cytometry. Events positive for red and green fluorescence were considered conjugates, and the percentage of conjugation was calculated as (red + green fluorescence/red fluorescence only) × 100. Data show mean ± SD of three independent experiments. Differences between groups were not significant. (G) Cell surface levels of CD11a and CD18 receptors remain unchanged in NK cells lacking Arl8b. YT-Indy cells (control or Arl8b shRNA transduced) were stained with isotype control, anti-CD11a-PE (left), or anti-CD18- fluorescein isothiocyanate (right) antibodies for 30 min on ice and analyzed by flow cytometry.

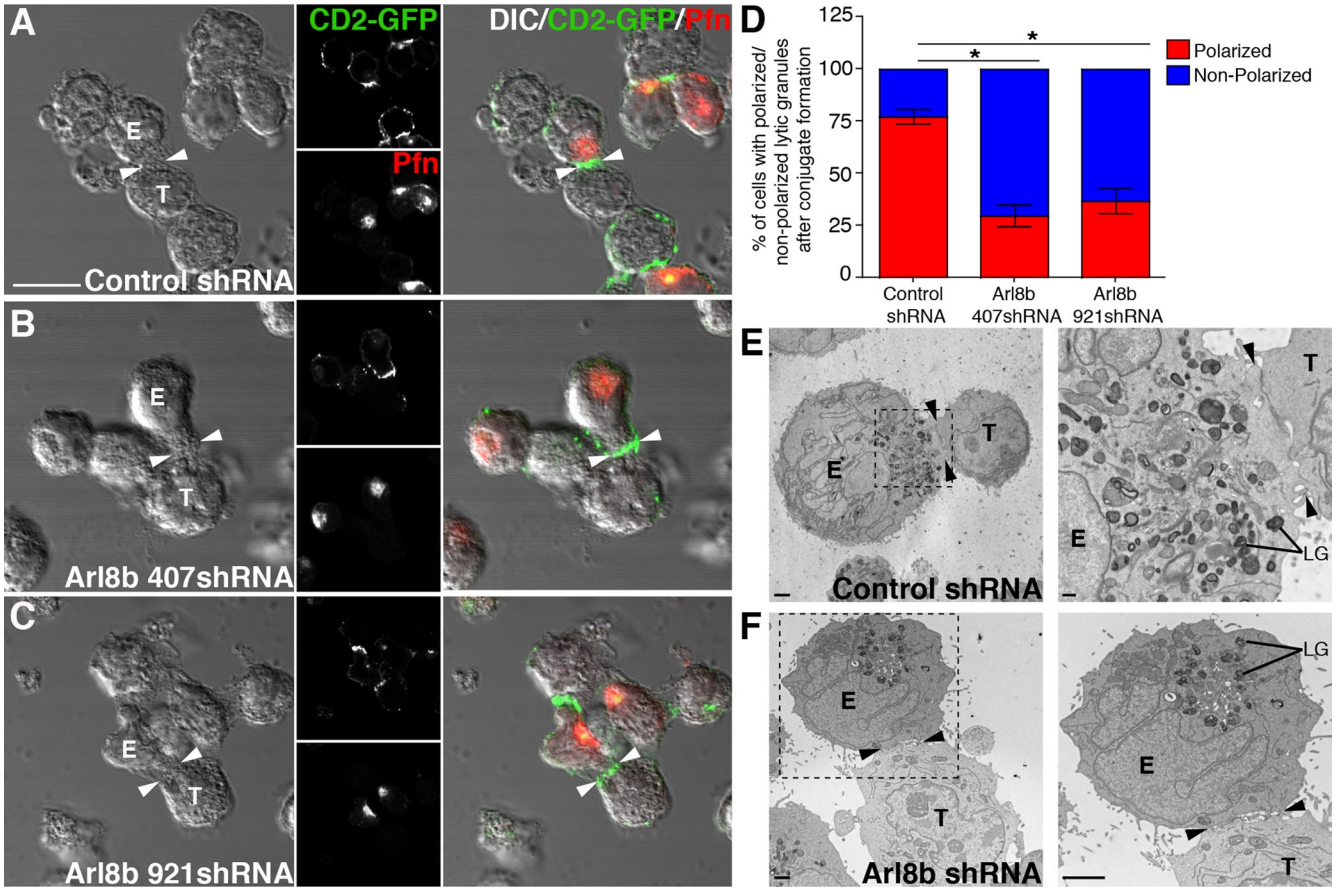

FIGURE 3: Ar8b is required for lytic granule polarization to the immune synapse in NK cells. (A–C) Lytic granules fail to polarize at the immune synapse in the absence of Arl8b. Confocal analysis was performed on YT-Indy-CD2-GFP cells (effector) stably transduced with control shRNA or Ar8b-specific shRNA (407 and 921) and mixed with 721.221 cells (target) for 20 min at the E:T ratio of 2:1. Conjugates were fixed, and lytic granules were stained using anti-perforin antibody (red). Immune synapse was identified in true conjugates by accumulation of CD2-GFP signal (white arrowhead). Scale bar, 10 μm. (D) The percentage of lytic granule polarization in control vs. Arl8b-silenced-YT-Indy cells. Bar graph, mean ± SD of three independent experiments; at least 100 conjugates were evaluated in each experiment. Asterisks indicate statistical significance (*$p < 0.05$ by Student's t test) as compared with control. (E, F) Transmission electron microscopy of control shRNA– or Arl8b shRNA–transduced YT-Indy cells (effector) incubated with 721.221 target cells (target). Black arrowhead, immune synapse; magnified boxed area highlights the presence of lytic granules (LGs) in close proximity to the immune synapse in conjugate between control shRNA–transduced YT-Indy cell and 721.221 target cell. Scale bar, 2 μm (E, left), 500 nm (E, right), and 2 μm (F, left and right). The analysis is based on evaluation of at least five conjugates in three separate experiments.

Several conjugates formed by control shRNA– or Arl8b shRNA–transduced YT-Indy cells were also visualized by transmission electron microscopy (EM). Arl8b silencing had no evident effect on either synapse formation or lytic granule morphology (Figure 3, E and F). However, consistent with our confocal microscopy analysis, lytic granules were docked away from the immune synapse in Arl8b-depleted cells but docked near the synapse in control cells (Figure 3, E and F, right). Thus Arl8b is specifically required for lytic granule polarization.

Arl8b is needed to orient the MTOC to the immune synapse

Lytic granule polarization is orchestrated by the reorientation of the MTOC to the immune synapse (Stinchcombe *et al.*, 2006, 2011). After NK cell activation, the lytic granules first rapidly converge to the MTOC and then move with the MTOC toward the immune synapse (Orange, 2008; Mentlik *et al.*, 2010; Kanwar and Wilkins, 2011; Sanchez-Ruiz *et al.*, 2011). In our analysis, the conjugates formed by Arl8b shRNA–transduced YT-Indy cells stained with pericentrin (to mark the MTOC) and perforin antibodies did not show any change in the convergence of lytic granules toward the MTOC compared with control conjugates (see later discussion of Figure 5A). To determine whether lack of Arl8b affects the subsequent stage—that is, MTOC polarization during synapse maturation—we analyzed control- and Arl8b shRNA–transduced YT-Indy cells in target cell conjugates. As expected, in control YT-Indy cells conjugated to 721.221 target cells, both the MTOC and the lytic granules polarized at the immune synapse (Figure 4A). Surprisingly, MTOC polarization failed to occur in Arl8b-silenced YT-Indy–target cell conjugates, and both the MTOC and the lytic granules remained away from the synapse (Figure 4, B and C). Analysis of >50 conjugates in three independent experiments of YT-Indy (control and Arl8b shRNA transduced) and 721.221 target cells after 20 min of incubation indicated that 81 ± 5% of conjugates formed by control shRNA–transduced cells showed MTOC polarization toward the immune synapse, whereas only 30 ± 8% of conjugates formed by Arl8b 407shRNA–transduced YT-Indy cells had polarized MTOC (Figure 4D). These results were

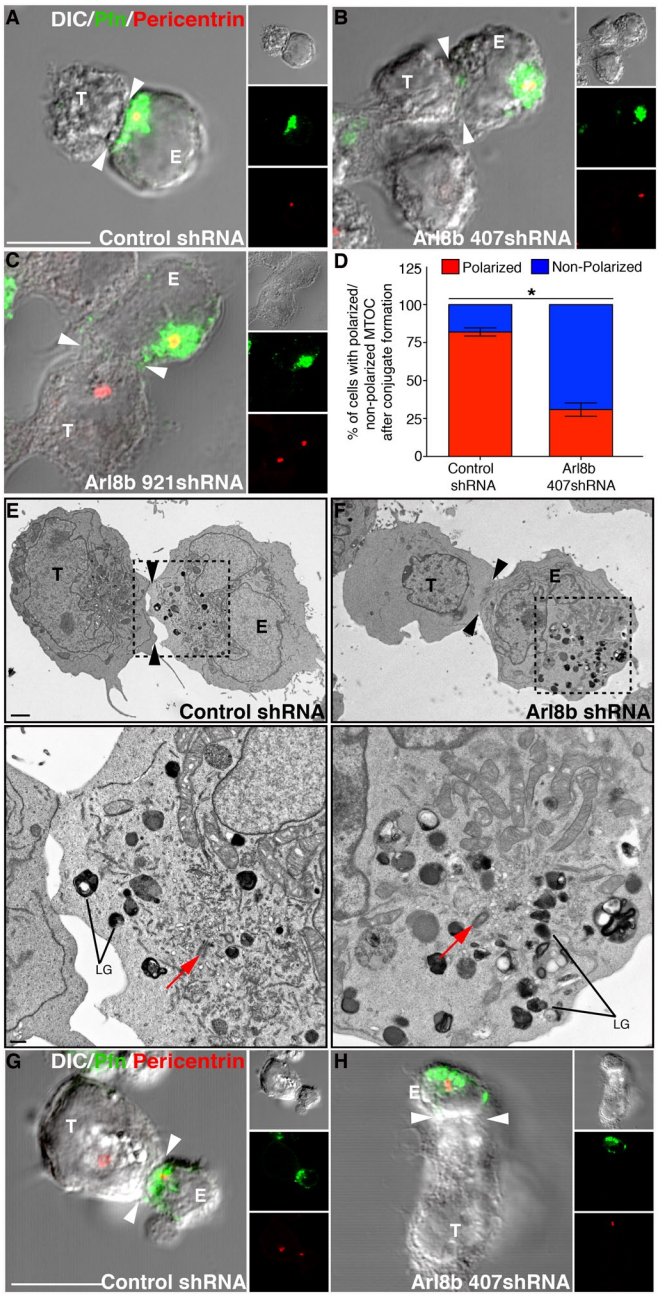

FIGURE 4: MTOC polarization to the immune synapse is inhibited in Arl8b-silenced NK cells. (A–C) Loss of MTOC polarization upon Arl8b silencing. Confocal analysis was performed on YT-Indy cells (effector) stably transduced with control shRNA or Ar8b-specific shRNA (407 and 921) and mixed with 721.221 cells (target) for 20 min at the E:T ratio of 2:1. Conjugates were fixed, and lytic granules were stained using anti-perforin antibody (green); the MTOC was determined based on pericentrin staining (red). Immune synapse is marked by white arrowhead. (D) Percentage of MTOC (marked by pericentrin staining) polarization in control vs. Arl8b-silenced-YT-Indy cells. Bar graph, mean ± SD of three independent experiments; at least 50 conjugates were evaluated in each experiment. Asterisks indicate statistical significance (*$p < 0.05$ by Student's t test) as compared with control. (E, F) Transmission electron microscopy of control shRNA– or Arl8b shRNA–transduced YT-Indy cells (E) incubated with 721.221 target cells (T). To better highlight the position of lytic granules (LGs) and MTOC (red arrow) in control vs. Arl8b-silenced NK cell–721.221 conjugates, the boxed area was magnified and is shown at the bottom. Black arrowheads indicate an immune synapse. Scale bar, 2 μm (top) and 500 nm (bottom). The analysis is based on evaluation of at least five conjugates in three separate experiments. (G, H) Control siRNA– and Arl8b siRNA–treated primary human NK cells (effector) were mixed with 721.221 cells (target) for 20 min at the E:T ratio of 2:1. Conjugates were fixed, costained for perforin (green) and pericentrin (red), and analyzed by confocal microscopy.

corroborated by transmission EM. Analyses of a number of NK–target cell conjugates indicated that the centrioles in Arl8b-silenced NK cells were unable to polarize in response to target cell recognition (Figure 4, E and F). As a control, we analyzed MTOC polarization to the immune synapse in Rab27a-depleted YT-Indy conjugates. Rab27a was shown to be involved during the later stage of docking and subsequent fusion of lytic granules in CTLs and predicted to play a similar role in NK cells. As expected, MTOC and lytic granules were polarized in Rab27a-knockdown NK cell conjugates but were still ineffective in killing the target cells (Figure 2E and Supplemental Figure S4C). These data support a model in which Arl8b acts before Rab27a in facilitating MTOC and lytic granule positioning at the immune synapse.

Because these assays were performed in transformed YT-Indy cells, we also tested whether these findings occurred in primary NK cells. Thus we isolated NK cells from human peripheral blood and silenced Arl8b expression using siRNA. Similar to our findings with the YT-Indy cell line, lytic granules and MTOC polarized in control siRNA–treated primary NK cell conjugates but not in Arl8b-silenced primary NK cells (Figure 4, G and H). Thus Arl8b regulates both MTOC and lytic granule positioning during NK cell cytotoxicity.

Impaired motility of lytic granules and the MTOC toward the immune synapse in Arl8b-silenced NK cells

To examine whether the failure of lytic granule and MTOC polarization in Arl8b-silenced NK cell conjugates is due to lack of their directional motility toward the immune synapse, we assessed the kinetics of lytic granule convergence to the MTOC and MTOC polarization in live cells using YT-Indy cells transfected to stably express green fluorescent protein (GFP)–tubulin and loaded with LysoTracker Red, which labels lytic granules, as well as lysosomes, in NK cells. In each conjugate, the distance between the MTOC and each LysoTracker-positive vesicle and the distance between the MTOC and the immune synapse were measured over 30 min. The MTOC was identified as an intense cluster of GFP-tubulin and lytic granules as intense clusters of LysoTracker Red–positive vesicles. To measure lytic granule convergence, we related the x, y coordinates of each lytic granule within the plane of the MTOC to the MTOC as described (Mentlik *et al.*, 2010). To measure MTOC polarization, we measured the distance between the MTOC and the immune synapse at each time point as described previously (Mentlik *et al.*, 2010).

First, we compared the distance of lytic granules from the MTOC in unconjugated and conjugated YT-Indy GFP-tubulin cells transduced with control or Arl8b shRNA. Before conjugation, Arl8b-silenced NK cells (blue line) exhibited more tightly converged lytic granules than control NK cells (red line), and this difference was significant (Figure 5, A and B). However, when Arl8b-silenced and control NK cells were allowed to conjugate to susceptible 721.221 target cells, lytic granule convergence to the MTOC led to no significant difference in the final distance of the lytic granules from the MTOC (Figure 5, A and B). Thus lack of Arl8b leads to clustering of lytic granules near the MTOC at steady state but does not have a discernible effect on their distance from the MTOC once the NK cell becomes activated. These findings are similar to the effect of Arl8b silencing on conventional lysosomes in other cell types, which leads

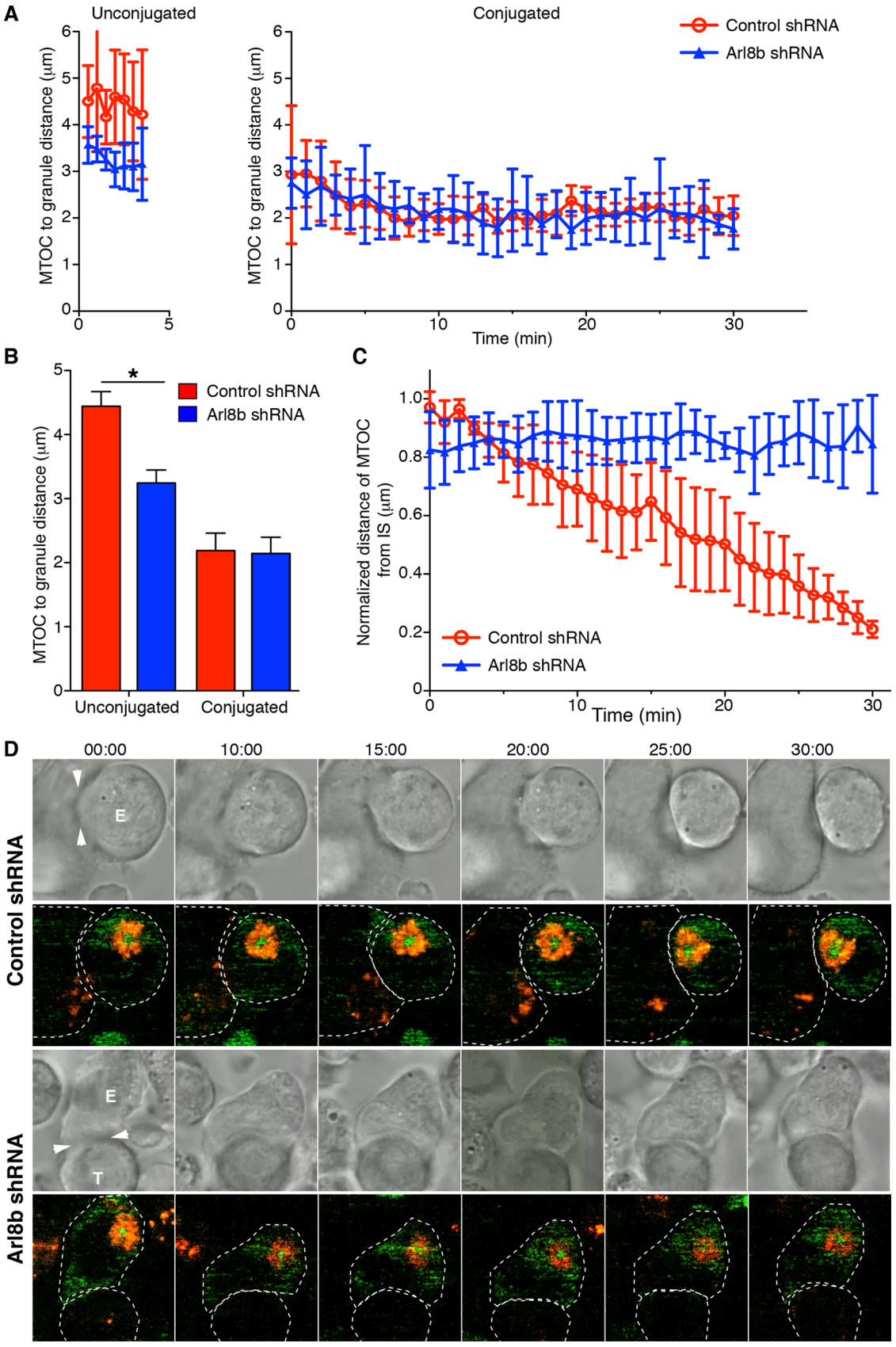

FIGURE 5: Dynamics of MTOC movement relative to the immune synapse and lytic granule movement in control vs. NK cells lacking Arl8b. (A, B) Quantitative analyses of lytic granule movement relative to the MTOC as measured by mean MTOC to granule distance ± SD as a function of time (left) or averaged over time (right) in unconjugated control or Arl8b-silenced cells and in conjugates between control or Arl8b-silenced NK cells and susceptible 721.221 target cells

to their accumulation near the MTOC (Hofmann and Munro, 2006; Garg *et al.*, 2011). We found that clustering of conventional lysosomes in HeLa cells lacking Arl8b depends on microtubule minus end–directed dynein motor (Supplemental Figure S5). In NK cells, the initial convergence of lytic granules to the MTOC also has been shown to depend on dynein (Mentlik *et al.*, 2010). Next, by using live-cell imaging, we compared the distance of the MTOC to the center of the immune synapse in control- or Arl8b-silenced YT-Indy cells conjugated to susceptible target cells. Although the MTOC moved to the synapse in control cells, the MTOC did not move closer to the synapse in Arl8b-silenced NK cell conjugates. For example, in one of the control shRNA–transduced YT-Indy conjugates, the normalized final MTOC-immune synapse distance was 0.17 µm, whereas in the case of Arl8b shRNA–transduced conjugate it was 0.90 µm. These results demonstrate unequivocally that Arl8b is required for MTOC and lytic granule polarization during NK cell cytotoxicity (Figure 5, C and D).

Kinesin-1 and its interaction partner SKIP are required for MTOC–lytic granule polarization toward the immune synapse to promote NK cell cytotoxicity

To investigate how Arl8b mediates MTOC and lytic granule motility toward the NK cell immune synapse, we sought to identify Arl8b-interacting proteins in NK cells. We therefore incubated YT-Indy cell lysate with immobilized glutathione *S*-transferase–tagged Arl8b (GST-Arl8b) and analyzed the bound proteins by mass spectrometry (Supplemental Figure S6). Not surprisingly, the dominant peptides corresponded to α/β-tubulin subunits, as previously reported for Arl8b pull down in HeLa cells (Garg *et al.*, 2011). We also recovered peptides from two HOPS complex subunits (Vps16 and Vps18), which were also previously found to associate with Arl8b. We also identified four unique peptides corresponding to KIF5B (the heavy chain of the plus-end motor protein kinesin-1 [KHC]) in the Arl8b pull down, which were not present in the GST control. Kinesin-1 is a heterotetramer of two KHC/KIF5B heavy chains and two kinesin light chains (KLCs). Kinesin-1 regulates long-range anterograde intracellular transport of vesicles, including lysosomes (Vale and Fletterick, 1997; Tanaka *et al.*, 1998). In particular, lysosomes have been shown to cluster around the MTOC in mouse cells lacking KHC/KIF5B (as we found in cells lacking Arl8b), suggesting a role of kinesin-1 in mediating the anterograde movement of lysosomes toward the cell periphery.

These findings suggested that KIF5B might mediate the effect of Arl8b on motility of both conventional lysosomes and lytic granules. To probe a potential role for KIF5B in motility of conventional lysosomes, we first compared the effect of knocking down Arl8b and KIF5B on the distribution of conventional lysosomes in HeLa cells. As previously reported, silencing of either gene led to similar perinuclear clustering of conventional lysosomes (Supplemental Figures 7, A–D; Tanaka *et al.*, 1998; Hofmann and Munro, 2006; Garg *et al.*, 2011). To examine whether Arl8b was required for KIF5B recruitment to lysosomes, we next overexpressed KIF5B-YFP in HeLa cells treated with control or Arl8b siRNA. Whereas KIF5B partially colocalized with endogenous LAMP-1 and Arl8b in control siRNA–treated cells (Figure 6A, inset), KIF5B was not recruited to lysosomes in Arl8b siRNA–treated cells (Figure 6B). These findings suggest that Arl8b helps recruit KIF5B to lysosomal membranes. In fact, a study (Rosa-Ferreira and Munro, 2011) described an interaction of Arl8b with SKIP, a protein that binds to the KLC of kinesin-1 and recruits the motor protein to lysosomal membranes to stimulate their plus end–directed motility.

We next investigated whether KIF5B interacts with Arl8b and regulates lytic granule polarization and NK cell cytotoxicity. To confirm interaction of Arl8b and KIF5B, we incubated purified wild-type (WT), dominant-active (Q75L), and dominant-negative (T34N) GST-Arl8b proteins with YT-Indy cell lysate and used GST-Arl3 and GST-purified proteins as controls. Immunoblotting of SDS–PAGE-resolved eluates with anti-KIF5B antibody showed a band in the GST-Arl8b lanes, but no pull down was observed with GST-Arl3 or GST only (Figure 6C). Even though the interaction with Arl8b was weak, it was consistently observed in several experiments (Figure 6D, quantification). Interestingly, in our experiments this interaction was found to be GTP-independent as no differences in KIF5B pull down were apparent when either the WT-, Q75L-, or T34N-Arl8b was used. We could not analyze the subcellular localization of KIF5B, as the antibody failed to recognize the endogenous protein in confocal microscopy analysis. Furthermore, our attempt to overexpress KIF5B in YT-Indy cells was not successful owing to the poor transfection efficiency of these cells.

Next, to identify the role of KIF5B in NK cell cytotoxicity, we stably transduced YT-Indy cells with control shRNA or KIF5B shRNAs (Supplemental Figure S7E), coincubated them with 721.221 target cells, and stained them with pericentrin and perforin antibodies. Silencing of KIF5B expression inhibited the polarization of both the MTOC and lytic granules to the immune synapse (Figure 6, E and F). This effect was further quantified in >100 conjugates of YT-Indy (control and KIF5B shRNA transduced) and 721.221 target cells stained with perforin antibody to mark lytic granules (Figure 6G). We next measured specific target killing by YT-Indy cells stably expressing two shRNAs against KIF5B or a control shRNA. Both KIF5B shRNAs dramatically reduced NK cell cytotoxicity as assessed by ^{51}Cr-release assay (Figure 6H).

Because a previous report described Arl8b association with kinesin-1 via linker protein SKIP (Rosa-Ferreira and Munro, 2011), we also investigated the role of SKIP in lytic granule and MTOC polarization in NK cells. The expression of SKIP was reduced in YT-Indy cells using two different shRNAs, and the silencing efficiency was measured by qRT-PCR (Figure 7E). To study the effect of SKIP silencing on lytic granule polarization, we coincubated YT-Indy cells stably transduced with control shRNA or SKIP shRNAs with 721.221 target cells and stained them with pericentrin and perforin antibodies. Silencing of SKIP expression significantly decreased the polarization of both the

($n = 5$ for all conditions). All mean distances of lytic granules from the MTOC were significantly less in conjugates from unconjugated NK cells ($p < 0.05$), and distance of lytic granules from the MTOC was significantly greater in control unconjugated NK cells than in Arl8b-silenced NK cells ($p < 0.05$). (C) Quantitative analyses of the mean distance ± SD between the MTOC and the immune synapse normalized to the largest distance of the MTOC from the immune synapse in that cell, as a function of conjugation time in conjugates between control NK cells and susceptible 721.221 target cells (red line) and Arl8b-silenced NK cells and susceptible 721.221 target cells (blue line). $n = 5$ for all conditions. (D) Time-lapse images of MTOC movement in (top) a YT-Indy GFP-tubulin cell transduced with control shRNA conjugated with a susceptible 721.221 target cell and (bottom) a YT-Indy GFP-tubulin cell transduced with Arl8b shRNA conjugated with a susceptible 721.221 target cell. In each pair of images, transmitted light is shown on the top and confocal immunofluorescence in the plane of the MTOC is shown on the bottom. Green fluorescence represents GFP–α-tubulin and red LysoTracker-loaded acidified organelles.

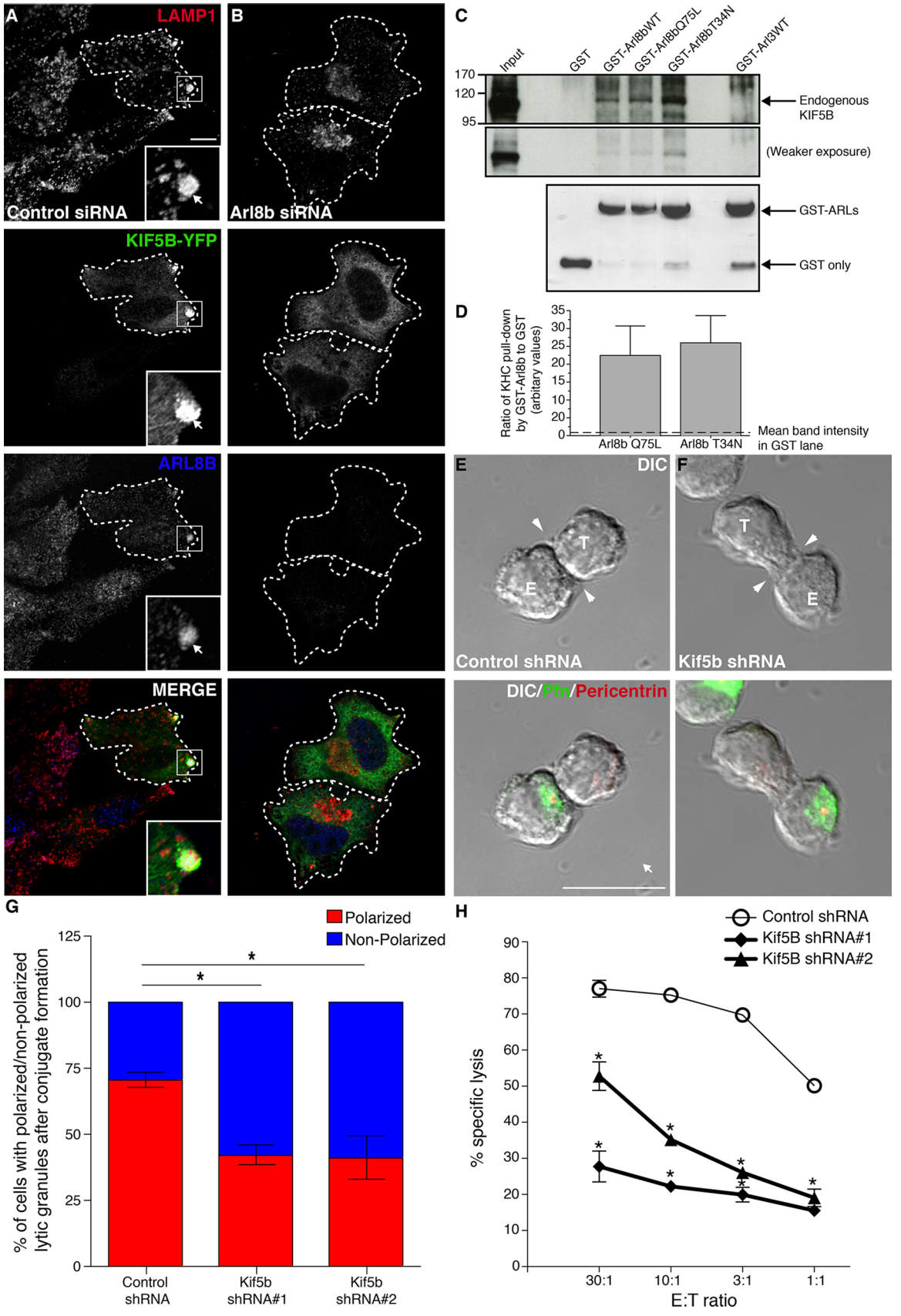

FIGURE 6: KIF5B, a kinesin motor protein recruited by Arl8b, regulates polarization of lytic granule–MTOC complex to the immune synapse in NK cells. (A, B) Arl8b is required for Kif5B localization to lysosomes. Control (A) or Arl8b siRNA–treated (B) HeLa cells were transfected with Kif5B-YFP. Post 24-h transfection, cells were fixed, costained with anti-Arl8b (blue) and anti–LAMP-1 (red) antibodies, and analyzed by confocal microscopy. The Kif5B-YFP–transfected

MTOC and lytic granules to the immune synapse (Figure 7, A–C; quantified in Figure 7D). SKIP-knockdown NK cell conjugates had lytic granules either polarized at the opposite end to that of the immunological synapse (as shown in Figure 7B) or randomly distributed throughout the cytoplasm (as shown in Figure 7C). Unfortunately, we were unable to confirm interaction of Arl8b and SKIP in YT-Indy cells due to a lack of antibody against SKIP that recognized the endogenous protein by Western blotting.

Our findings provide the first evidence suggesting that kinesin-1 is a critical motor protein, which, along with Arl8b and SKIP, is required to move the MTOC- lytic granules to the immune synapse during NK cell lysis.

DISCUSSION

In this study, we define a new role for the small GTP-binding protein Arl8b in regulating motility and exocytosis of lytic granules of NK cells. Previously, Arl8b was shown to regulate the motility of conventional lysosomes on microtubule tracks and thereby control their spatial distribution within the cytosol (Bagshaw *et al.*, 2006; Hofmann and Munro, 2006; Rosa-Ferreira and Munro, 2011). Previous proteomics studies also suggested that Arl8b is present on the surface of several LROs (Casey *et al.*, 2007; Hu *et al.*, 2007), suggesting that Arl8b might also regulate motility of cytolytic granules on microtubule tracks during their polarization and exocytosis. Using NK cells as a model system, we demonstrate that Arl8b localizes to lytic granules and is required for NK cell cytotoxicity. Arl8b silencing did not alter the initial stages of NK–target cell adhesion and conjugate formation but interfered with the mobilization of the MTOC and granules to the immune synapse. MTOC polarization is a crucial step in lymphocyte cytotoxicity for delivery of the contents of lytic granules to the surface of target cells (Stinchcombe *et al.*, 2006; Orange, 2008). Of interest, several reports indicate that both in resting and target cell–conjugated primary NK cells and NK cell lines, polarization of lytic granules toward the immune synapse is most probably simultaneous to and driven by MTOC polarization (Orange *et al.*, 2003; Stinchcombe *et al.*, 2006, 2011; Mentlik *et al.*, 2010; Kanwar and Wilkins, 2011). We found that not only lytic granules, but, surprisingly, also the MTOC was unable to polarize toward the immune synapse in Arl8b-depleted NK cells. Our findings for the first time reveal that lytic granule–MTOC movement depends on Arl8b.

We also identified KIF5B, the heavy chain of the plus-end motor protein kinesin-1, as an Arl8b binding partner. SKIP was identified as a protein that links Arl8b to kinesin-1 to recruit the motor protein to conventional lysosomal membranes (Rosa-Ferreira and Munro, 2011). We found that similar to Arl8b knockdown, depletion of both kinesin-1 and SKIP in NK cells results in lack of MTOC and lytic granule polarization at the immune synapse. In this study, we did not investigate whether Arl8b and KIF5B are required for cytolytic granule movement and killing by CTLs. Kinesin-1 was reported to mediate the terminal transport of polarized lytic granules from the MTOC to the immune synapse in CTLs (Kurowska *et al.*, 2012). However, in CTLs, the small GTP-binding protein Rab27a and its effector Slp3 were shown to recruit kinesin-1 to lytic granules. CTL granules acquire Rab27a by fusing with exocytic vesicles at a late stage of granule exocytosis after granules moved with the MTOC to the vicinity of the immune synapse. This fusion event is a prerequisite for CTL granules to dock at the plasma membrane. Like CTLs, Rab27a depletion in NK cells also arrests lytic granules at a subsequent docking step during granule release (Haddad *et al.*, 2001; Stinchcombe *et al.*, 2001). It will be interesting to analyze the role of kinesin-1 in NK cell lytic granule docking, also possibly mediated by its binding to the small GTPase Rab27a and its effector.

We propose a model in which Arl8b GTPase and its interaction partner kinesin-1 may first orchestrate movement of the MTOC in the first phase of granule mobilization, escorting its microtubule-bound granules with it. In fact, Arl8b silencing does not affect the distance of the granules from the MTOC (Figure 5, A and B), which is probably mediated by a "minus end"–directed dynein-dependent motor. Once close to the plasma membrane at the immune synapse, Arl8b and/or Rab27a might then recruit the plus-end kinesin-1 motor, probably via adaptors, to move the granules along the microtubules from the MTOC to dock at the plasma membrane. Future studies are needed to define the roles of Arl8b and Rab27a during granule mobilization and identify the adaptors at work at each step in the process. It would be useful if NK cell and T-cells were studied in parallel to determine whether apparent differences in mobilization of lytic granules are at work.

cell is marked with dashed white boundary, and the inset shows colocalization between Kif5B-YFP, endogenous Arl8b, and lysosome marker, LAMP-1. Scale bar, 10 µm. (C, D) Arl8b associates with Kif5B in YT-Indy cells. Bacterially expressed, purified recombinant GST-Arl8b (WT), GST-Arl8b (Q75L), GST-Arl8b (T34N), GST-Arl3 (WT), or GST only was incubated with lysates from YT-Indy cells. The bound proteins were resolved by SDS–PAGE, transferred to PVDF, and immunoblotted with anti-Kif5B antibody (top). A weaker exposure (middle) was taken to better visualize the Kif5B signal in the input lane. For the assay, all the purified proteins were taken in equal amounts as shown at the bottom. The graph in D represents densitometric analyses performed on three independent experiments. Briefly, the ratios of band intensity of Kif5B pulled down by GST-Arl8b (Q75L) and GST-Arl8b (T34N) to that of GST-only were calculated in each experiment. Note that the actual numerical values for ratios of Kif5B band intensity varied with each experiment; for GST-Arl8b (Q75L) to GST they produced values of 37, 8.4, and 22, and for GST-Arl8b (T34N) to GST they yielded values of 36, 11, and 31. However, as these values are arbitrary in nature (depending on film exposure times, etc.), by comparing Arl8b to GST in each individual experiment, it was possible to normalize GST value at 1 (see dotted line in bar graph) and represent a mean fold increase in Kif5B pull down by Arl8b (Q75L) and Arl8b (T34N) for all three experiments (including SE bars). No significant difference was observed between Kif5B pulled down by GST-Arl8b (Q75L) or GST-Arl8b (T34N). (E–G) Kif5B is required for lytic granule–MTOC complex polarization to immune synapse in NK cells. Confocal analysis was performed on YT-Indy cells stably transduced with control shRNA or Kif5B-specific shRNA (#1 and #2) and mixed with 721.221 target cells for 20 min at the E:T ratio of 2:1. Conjugates were fixed, lytic granules were stained using anti-perforin antibody (green), and the MTOC was marked by anti-pericentrin antibody staining (red). (G) The percentage of lytic granule polarization in control vs. Kif5B-silenced YT-Indy cells. Bar graph, mean ± SD of three independent experiments; at least 100 conjugates were evaluated in each experiment. Asterisks indicate statistical significance (*$p < 0.05$ by Student's *t* test) as compared with control. (H) Silencing of Kif5B reduces NK cell cytotoxicity. YT-Indy cells were stably transduced with control shRNA or Kif5B-specific shRNAs (shRNAs #1 and #2), and their ability to kill 721.221 target cells was measured by ^{51}Cr-release assay at various E:T ratios. Data show mean ± SEM from triplicates of one representative experiment of three performed; *$p < 0.05$.

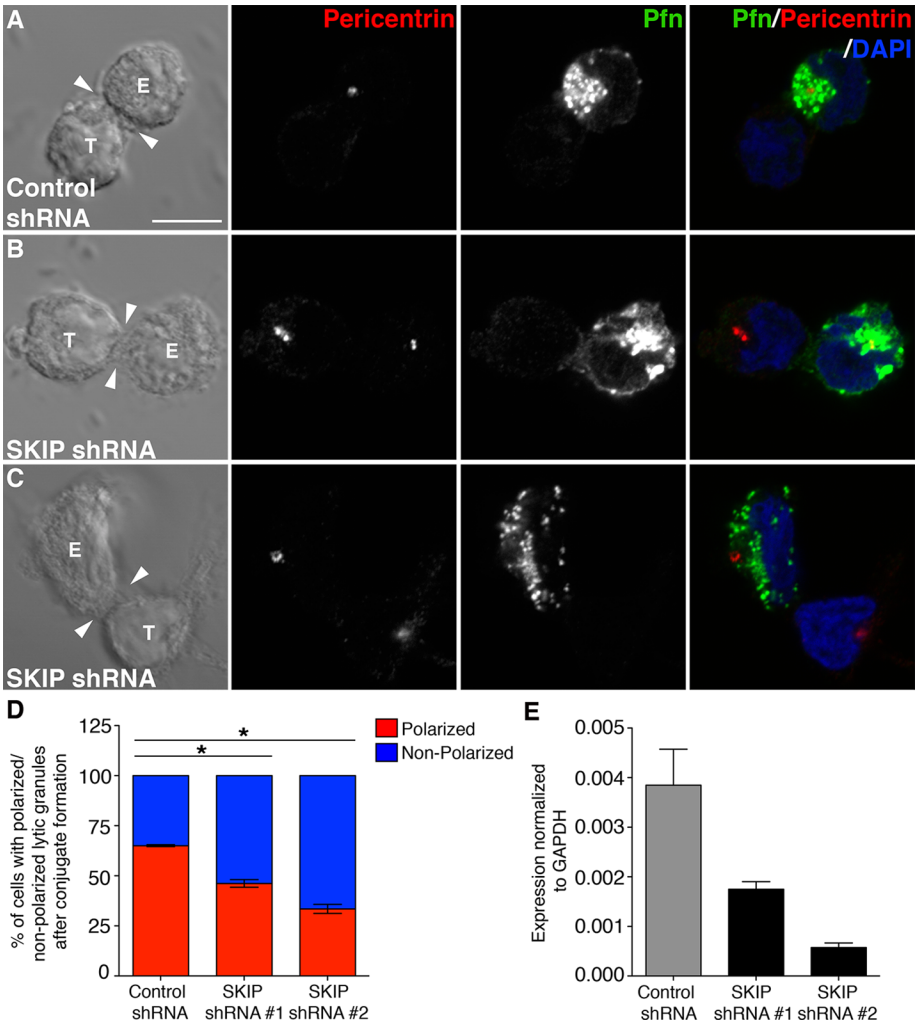

FIGURE 7: Lytic granule–MTOC complex polarization to the immune synapse is inhibited in SKIP-silenced NK cells. (A–C) SKIP is required for lytic granule–MTOC complex polarization to immune synapse in NK cells. Confocal analyses was performed on YT-Indy cells stably transduced with control shRNA or SKIP-specific shRNA and mixed with 721.221 target cells for 20 min at the E:T ratio of 2:1. Conjugates were fixed, lytic granules were stained using anti-perforin antibody (green), and the MTOC was marked by anti-pericentrin antibody staining (red). (D) The percentage of lytic granule (marked by perforin staining) polarization in control vs. SKIP-silenced YT-Indy cells. Bar graph, mean ± SD of three independent experiments; at least 50 conjugates were evaluated in each experiment. Asterisks indicate statistical significance (*$p < 0.05$ by Student's t test) as compared with control. (E) Silencing of SKIP in YT-Indy cells. Stable silencing of SKIP was achieved in YT-Indy cells by introducing lentiviral vector–driven shRNA against SKIP (shRNAs #1 and #2), and qRT-PCR was performed to check the efficiency of SKIP silencing.

How the concerted action of Arl8b and kinesin-1 generates the force required for the MTOC movement/polarization to the immune synapse remains unclear. Previous studies described only the signaling pathways required for MTOC polarization. For instance, extracellular-signal-regulated kinase phosphorylation, VAV1 activation, and protein tyrosine kinase 2 activity are required for MTOC polarization in NK cells (Sancho *et al.*, 2000; Graham *et al.*, 2006; Chen *et al.*, 2007). Similarly in CTLs, T-cell receptor signaling and activity of a small GTPase of the Rho subfamily, cell division cycle 42, is required for MTOC polarization (Stowers *et al.*, 1995; Lowin-Kropf *et al.*, 1998). How such signaling pathways cross-talk with the motor proteins or motor-associated proteins to result in MTOC polarization is a key question. It will also be interesting in this context to analyze the role of Arl8b in regulating the dynamics of the microtubule network. It was shown that microtubule dynamics plays a critical role in NK cell cytotoxicity, as pharmacologic inhibition of microtubule dynamics blocks granule polarization and target cell lysis (Orange *et al.*, 2003; Graham *et al.*, 2006). Arl8b was shown to bind to α- and β-tubulin subunits, as well as to polymerized microtubules, in an in vitro assay (Okai *et al.*, 2004). Moreover, we found the maximum number of peptides of α/β-tubulin in all our mass spectrometry screenings using GST-Arl8b as the bait to pull down interaction partners from YT-Indy cell lysates. The significance of this interaction and whether indeed Arl8b can directly regulate MTOC movement by influencing the assembly and disassembly of the microtubule network are among the questions that remain to be answered. Given the findings that the biogenesis and exocytosis of various LROs uses common machinery, it will important to address the role of Arl8b and its effectors in regulating the activity of other specialized LROs and granules, as many other important functions are likely to be dependent on Arl8b.

MATERIALS AND METHODS

Cell lines

The immortalized human NK cell line YT-Indy was used as a model NK cell system, and 721.221 cells were used as a susceptible target cells for YT-Indy cells. These cells were cultured in RPMI (Life Technologies, Grand Island, NY) 37°C, 5% CO_2 supplemented with 10% fetal bovine serum (Hyclone, Waltham, MA), 2 mM L-glutamine, 100 U/ml penicillin, 100 μg/ml streptomycin, sodium pyruvate, and 10 mM 4-(2-hydroxyethyl)-1-piperazineethanesulfonic acid. YT-Indy cells stably expressing GFP–α-tubulin and CD2-GFP (a kind gift from Jordan Orange, Baylor College of Medicine, Houston, TX) were maintained as described previously (Mentlik *et al.*, 2010). Primary human NK cells were isolated from whole blood obtained from volunteer donors by negative depletion using the human NK cell isolation kit (Miltenyi Biotec, Auburn, CA). HeLa cells were cultured in DMEM (Life Technologies) with the aforementioned supplements.

Antibodies

The following antibodies were used in this study: rabbit polyclonal antibody against Arl8 (Garg *et al.*, 2011); rabbit anti-actin (Sigma-Aldrich, St. Louis, MO); rabbit anti-pericentrin (Abcam, Cambridge, MA); rabbit anti-Kif5b (Santa Cruz Biotechnology, Dallas, TX); mouse anti-perforin (Pfn), clone Pf80/164 (Mabtech, Mariemont, OH); mouse anti-Pfn, clone Pf344 (Mabtech); mouse anti-GzmB, clone GB10 (Mabtech); mouse anti-GzmB, clone GB11 (Caltag Laboratories, Camarillo, CA); mouse anti-GzmB, clone GrB7

(Sigma-Aldrich); mouse anti-CD18, clone TS1/18 (Biolegend, San Diego, CA); mouse anti–Lamp-1, clone H4A3 (BD PharMingen, San Jose, CA); mouse anti-CD48, clone TU145 (BD PharMingen); mouse anti-EEA1 (BD Biosciences, San Jose, CA); mouse anti–β-actin, clone AC-74 (Sigma-Aldrich); and mouse anti-CD11α, clone TS1/22 (Thermo Scientific, Waltham, MA). Secondary goat anti-mouse Alexa 488, goat anti-mouse Alexa 568, goat anti-rabbit Alexa 488, and goat anti-rabbit Alexa 568 antibodies were purchased from Invitrogen (Grand Island, NY). Goat anti-mouse horseradish peroxidase (HRP) and goat anti-rabbit HRP antibodies were purchased from Jackson ImmunoResearch Laboratories (West Grove, PA).

Lentiviral shRNA–mediated silencing

All lentiviruses were produced in accordance with protocols publicly available at the Broad Institute's RNAi Consortium Web site (www.broadinstitute.org). For lentiviral transduction, YT-Indy, YT-Indy–CD2-GFP, or YT-Indy–α-tubulin cells were plated in 96-well round-bottom plates (15,000 cells/well; Corning) in Polybrene (8 µg/ml; Sigma-Aldrich) and mixed with 10 µl of viral supernatant (day 0). Puromycin (Sigma-Aldrich) was added after 24–48 h at 5 µg/ml for a minimum of 3 d to select transductants, and experiments were performed on days 5–20 after transduction. shRNA target sequences were as follows: Mission (negative control sequence), CAACAAGATGAAGAGCACCAA; Arl8a 497, CTCCACAACCTACTGGACAAA; Arl8a 1685, GCTCATATTTAACCTCTGTTT; Arl8b 407, AGGTAACGTCACAATAAAGAT; Arl8b 921, GCTGAAGATGAATATCCCTAA; Kif5b shRNA #1, GCCCTATTTATTACACAGTTT; Kif5b shRNA #2, CGGAACACTATTCAGTGGCTT; SKIP shRNA #1, CAATGGACTTCTACCGCTTTA; SKIP shRNA #2, TGAAGTCAGCCATGATCAAAG; and Rab27a shRNA, CCTGTGCATTTGAATTGTATA.

Gene silencing by siRNA

siRNA duplexes for Arl8b (synthesized by Dharmacon) were transfected in HeLa cells using Dharmafect 1 (Dharmacon, Pittsburgh, PA) as previously described for 72 h. On-Target SMART pool from Dharmacon was used for dynein heavy chain 1 (L-006828-00-0005) and Kif5b (L-008867-00-0005). Isolated primary human NK cells were nucleofected with siRNA using an Amaxa Nucleofector with program O-017 and the human cell reagent (Amaxa, Basel, Switzerland) in accordance with the manufacturer's instructions. The nucleofected cells were cultured for 72 h before use.

qRT-PCR

Total RNA from cells lysed using QIAshredder columns (Qiagen, Valencia, CA) was extracted with the RNeasy Mini Kit (Qiagen) in accordance with the manufacturer's instructions. cDNA was synthesized with the QuantiTect Reverse-Transcription Kit (Qiagen) in accordance with the manufacturer's instructions. Quantitative PCR was performed using Brilliant SYBR Green QPCR Master Mix (Agilent Technologies, Santa Clara, CA) on an Mx3000P QPCR System (Agilent Technologies). Transcript in each sample was assayed in triplicate, and the mean cycle threshold was used to calculate the expression level relative to glyceraldehyde-3-phosphate dehydrogenase (GAPDH) housekeeping gene. The primers used were as follows: 5′-AGTCCTGGGTAACAAGCGAGAC-3′ (sense) and 5′-GCAAGAGATGGAGTAGCAGCAG-3′ (antisense) for Arl8a; 5′-CACCTTCGTCAATGTCATCG-3′ (sense) and 5′-CCTATGTCCCAGATCTTTATTGTG-3′ (antisense) for Arl8b; 5′-AACAGTGGGCATTGATTTCAG-3′ (sense) and 5′-CTCCAGATCACTCTTGTTTCC-3′ (antisense) for Rab27a; 5′-GAGTTAGCAGCATGTCAGCTTCG-3′ (sense) and 5′-GCATCGACAGATTCCTCCAACTG-3′ (antisense) for Kif5b; 5′-CCGAGAAAACGAAGAGCAGCTG-3′ (sense) and 5′-TCCACCAGGTATGGCTTCTCTG-3′ (antisense) for SKIP; and 5′-CATTTCCTGGTATGACAACGA-3′ (sense) and 5′-GTCTACATGGCAACTGTGAG-3′ (antisense) for GAPDH.

Fixed-cell confocal microscopy

NK cells (control or shRNA transduced) alone or conjugated to 721.221 target cells at a ratio of 2:1 for 20 min at 37°C were adhered to 0.1% poly-L-lysine–coated glass slides (PolyPrep; Sigma-Aldrich) by gentle centrifugation at 900 rpm for 3 min. After the indicated time, cells were fixed for 10 min in phosphate-buffered saline (PBS) with 4% paraformaldehyde (PFA; Electron Microscopy Sciences, Hatfield, PA), washed, and incubated 10 min in PBS with 50 mM NH_4Cl. Cells were then washed with PBS and permeabilized for 5 min in permeabilization buffer (PBS, 0.2% Triton X-100). After two washes in PBS, coverslips were placed in blocking solution (PBS, 10% fetal calf serum) for 30 min, washed once in PBS, and incubated for 1 h with the indicated primary antibodies in incubation buffer (PBS, 0.05% Triton X-100). Cells were then washed three times with incubation buffer and incubated for 30 min each with the indicated secondary antibodies in incubation buffer. Cells were mounted in Fluoromount G (Southern Biotech, Birmingham, AL) and imaged on a Nikon TE2000-U inverted microscope equipped with the laser scanning C1 confocal system.

Live-cell confocal microscopy

MTOC polarization to the immune synapse and lytic granule convergence to the MTOC were quantitatively measured as described for live-cell experiments (Mentlik *et al.*, 2010). Briefly, GFP–α-tubulin–expressing YT-Indy cells transduced with either control or Arl8b shRNA were suspended in media at a concentration of 3×10^6 cells/ml, incubated with 5 µM LysoTracker Red DND-99 (Molecular Probes, Grand Island, NY) for 30 min at 37°C, washed, and resuspended in media at 3×10^6 cells/ml. 721.221 cells were suspended in media at a concentration of 4×10^5 cells/ml and adhered for 30 min at 37°C to ΔT dishes (Bioptechs, Butler, PA) precoated with antibodies against CD48 (BD PharMingen), after which NK cells were added. Conjugates were imaged every 10 s for 30 min in a single *z*-axis plane using a Zeiss Axio Observer Z1 outfitted with Yokogawa CSU10 spinning disk, Hamamatsu Orca-AG camera, and Zeiss 63×/1.43 numerical aperture oil immersion objective. The Zeiss system used solid-state 488- and 561-nm lasers (Crystal) managed through an LMM5 laser combiner unit (Spectral Imaging). In all live-cell experiments, temperature was maintained at 37°C using ΔT dish and objective environmental control units (Bioptechs). Image sequences were then analyzed using Volocity software (PerkinElmer, Waltham, MA). For analysis, unadjusted images were measured for fluorescence corresponding to the MTOC (GFP maximal intensity) or lytic granules (LysoTracker Red maximal intensity), and regions of positivity were selected based on two to five SDs above mean intensity. In time-lapse experiments, at least 1 image/min was used for quantitative analysis. To measure distance between the MTOC and immune synapse, a line connecting the center of the immune synapse to the MTOC was drawn using Volocity software. Because the distances between the MTOC and the immune synapse varied significantly between cells, these values were normalized as follows: distance between the MTOC and the immune synapse was measured in each time frame, and each value was divided by the furthest distance between the MTOC and immune synapse in that cell. In this way, initial normalized distance was approximately 1, and as the MTOC approached the immune synapse, the normalized distance became a fraction of 1. To measure distance between the MTOC and lytic granules, *x* and *y* coordinates of the MTOC and all

lytic granules in the plane of the MTOC were obtained. Distance between the MTOC and lytic granules was determined as described (Mentlik *et al.*, 2010). For statistical analysis, the minimum number of cells evaluated was determined using sample size calculations based up preliminary data, with α and β error levels of 1%. Differences over time between Arl8b shRNA and control shRNA NK cells, conjugated and unconjugated, were evaluated using unpaired Mann–Whitney *U* tests. Differences were considered significant when $p \leq 0.05$.

Electron microscopy

Conjugates between NK and target cells at a 2:1 ratio were formed in suspension for 20 min at 37°C and subsequently adhered on plastic coverslip (precoated with 0.1% poly-L-lysine) placed in a 12-well dish by centrifugation at 900 rpm for 3 min. Cells were fixed (in the dish) in routine fixative (2.5% glutaraldehyde/1.25% PFA/0.03% picric acid in 0.1 M sodium cacodylate buffer, pH 7.4) for at least 1 h at room temperature and washed in 0.1 M sodium cacodylate buffer (pH 7.4). The cells were then postfixed for 30 min in 1% osmium tetroxide/1.5% potassium ferrocyanide, washed in water three times, and incubated in 1% aqueous uranyl acetate for 30 min, followed by two washes in water and subsequent dehydration in grades of alcohol (5 min each: 50, 70, 95, 2× 100%). Cells were removed from the dish in propylene oxide, pelleted at 3000 rpm for 3 min, and infiltrated for 2 h to overnight in a 1:1 mixture of propylene oxide and TAAB Epon (Marivac Canada). The samples subsequently embedded in TAAB Epon and polymerized at 60°C for 48 h. Ultrathin sections were cut on a Reichert Ultracut-S microtome, picked up onto copper grids stained with lead citrate, and examined in a JEOL 1200EX transmission electron microscope. Images were recorded with an AMT 2k charge-coupled device camera.

Chromium release assay

Cytotoxicity was measured by 4-h chromium release assay. Briefly, ^{51}Cr-labeled target cells were incubated for 4 h at 37°C with effector cells at different effector/target ratios in a final volume of 200 µl in 96-well microplates. Experiments were performed in triplicate. At the end of the incubation 50 µl of the supernatant was transferred into 96-well LumaPlate solid scintillation plates (Packard Instrument, Waltham, MA) and counted in a Top Count counter (Packard Instrument) after overnight drying. Data are expressed as percentage of specific ^{51}Cr release from target cells, calculated as (experimental release − spontaneous release)/(maximum release − spontaneous release) × 100.

Fluorescence-activated cell sorting–based conjugation assay

NK–target cell conjugate formation was measured by cytometry as described previously. YT-Indy cells (control or Arl8b shRNA transduced) and target cells (721.221) were stained with PKH26 (Red Fluorescent Cell Linker; Sigma-Aldrich) and PKH67 (Green Fluorescent Cell Linker; Sigma-Aldrich), respectively. Labeled cells were coincubated at a 2:1 E:T ratio for 20 min, fixed in 4% PFA, and analyzed by flow cytometry. Events positive for red and green fluorescence were considered conjugates, and the percentage of conjugation was calculated as (red + green fluorescence/red fluorescence only) × 100.

F-actin polymerization assay

To visualize F-actin accumulation at immunological synapse, YT-Indy cells stably transduced with control shRNA or Arl8b shRNA were mixed with anti-LFA1 monoclonal antibody–coated polystyrene beads (6.7–8.0 µm diameter; Spherotech, Lake Forest, IL) for 1 h at 37°C. After mixing with the beads, cells were fixed, permeabilized, and stained with Alexa Fluor 488–conjugated phalloidin (Invitrogen) to visualize polymerized F-actin by confocal microscopy as described.

GST pull-down assay

GST pull-down assay from NK cells followed by mass spectrometry was performed as described previously (Garg *et al.*, 2011). Briefly, YT-Indy cell lysates prepared in 0.5% 3-[(3-cholamidopropyl) dimethylammonio]-1-propanesulfonate buffer were incubated with purified GST-Arl8b or GST for 2 h. Eluates were run on SDS–PAGE, and protein bands that appeared specifically in the GST-Arl8b lane were cut, partially digested, and analyzed by mass spectrometry. For KHC pull down, bacterially expressed, purified recombinant GST-Arl8b (WT), GST-Arl8b (Q75L), GST-Arl8b (T34N), GST-Arl3 (WT), or GST only was incubated with lysates from YT-Indy cells. The bound proteins were resolved by SDS–PAGE, transferred to polyvinylidene fluoride (PVDF), and immunoblotted with anti-Kif5B antibody.

Isolation of lytic granules from NK cells

Lytic granules were prepared from 3×10^8 YT-Indy cells as previously described (Mentlik *et al.*, 2010). Briefly, cells were lysed and homogenized using a Dounce homogenizer. The homogenized lysates were subjected to centrifugation at $1000 \times g$ to remove the nuclei. The postnuclear lysate was subjected to centrifugation at $18{,}000 \times g$ to pellet the lytic granules, yielding the crude lysosomal fraction (CLF). The CLF was resuspended in extraction buffer and subjected to density gradient ultracentrifugation at $150{,}000 \times g$ on an 8–27% OptiPrep gradient (Lysosome Enrichment Kit; Pierce, Rockford, IL), and seven fractions (1–7) of 0.53 ml each were harvested for further analysis.

Immunoblotting

Lysates from NK cells or HeLa cells were made in 0.5% Triton X-100 lysis buffer. Protein concentration in cell lysates was determined using the Bradford kit (Bio-Rad, Hercules, CA), and equal amounts of each sample were analyzed on precast 4–20% SDS–PAGE (Invitrogen) and transferred to PVDF membranes (Invitrogen). Membranes were blocked with blocking buffer (10% skim milk and 0.1% Tween-20 in PBS) overnight and incubated the next day with the indicated primary antibody, followed by incubation with corresponding HRP-conjugated secondary antibody (Jackson ImmunoResearch Laboratories). Blots were developed with ECL/Pico reagent (Pierce) and exposed to Kodak Bio-Max film (Eastman Kodak, Waltham, MA) for visualization of the bands.

ACKNOWLEDGMENTS

We thank S. Linder (Universitätsklinikum Hamburg-Eppendorf, Hamburg, Germany), K. Verhey (University of Michigan, Ann Arbor, MI), and T. Schroer (Johns Hopkins University, Baltimore, MD) for their general gifts of molecular constructs. We thank M. Ericsson for help in electron microscopy analyses, M. Walch for assistance in chromium assay, and R. Tomaino for assistance with mass spectrometry (Taplin Biological Mass Spectrometry Facility, Harvard Medical School, Boston, MA). A.T. thanks J. Solheim, S. Caplan, and N. Naslavsky (University of Nebraska, Lincoln, NE) for their previous mentorship, gifts of molecular constructs, and helpful discussions and critical reading of the manuscript and members of the Brenner, Jordan, and Lieberman laboratories and V. Hsu for helpful discussions. A.T. acknowledges support from a Ramanujan Fellowship (Department of Science and Technology, India). M.S. is the recipient of a Wellcome Trust/DBT India Alliance Intermediate Fellowship Award and acknowledges support from a Wellcome Trust grant.

REFERENCES

Bagshaw RD, Callahan JW, Mahuran DJ (2006). The Arf-family protein, Arl8b, is involved in the spatial distribution of lysosomes. Biochem Biophys Res Commun 344, 1186–1191.

Benado A, Nasagi-Atiya Y, Sagi-Eisenberg R (2009). Protein trafficking in immune cells. Immunobiology 214, 507–525.

Bonifacino JS (2004). Insights into the biogenesis of lysosome-related organelles from the study of the Hermansky-Pudlak syndrome. Ann NY Acad Sci 1038, 103–114.

Burkhardt JK, Hester S, Lapham CK, Argon Y (1990). The lytic granules of natural killer cells are dual-function organelles combining secretory and pre-lysosomal compartments. J Cell Biol 111, 2327–2340.

Casey TM, Meade JL, Hewitt EW (2007). Organelle proteomics: identification of the exocytic machinery associated with the natural killer cell secretory lysosome. Mol Cell Proteomics 6, 767–780.

Chen X, Trivedi PP, Ge B, Krzewski K, Strominger JL (2007). Many NK cell receptors activate ERK2 and JNK1 to trigger microtubule organizing center and granule polarization and cytotoxicity. Proc Natl Acad Sci USA 104, 6329–6334.

Dell'Angelica EC, Mullins C, Caplan S, Bonifacino JS (2000). Lysosome-related organelles. FASEB J 14, 1265–1278.

Donaldson JG, Jackson CL (2011). ARF family G proteins and their regulators: roles in membrane transport, development and disease. Nat Rev Mol Cell Biol 12, 362–375.

Echard A, Jollivet F, Martinez O, Lacapere JJ, Rousselet A, Janoueix-Lerosey I, Goud B (1998). Interaction of a Golgi-associated kinesin-like protein with Rab6. Science 279, 580–585.

Fukuda M (2006). Rab27 and its effectors in secretory granule exocytosis: a novel docking machinery composed of a Rab27.effector complex. Biochem Soc Trans 34, 691–695.

Fukuda M, Kuroda TS, Mikoshiba K (2002). Slac2-a/melanophilin, the missing link between Rab27 and myosin Va: implications of a tripartite protein complex for melanosome transport. J Biol Chem 277, 12432–12436.

Garg S, Sharma M, Ung C, Tuli A, Barral DC, Hava DL, Veerapen N, Besra GS, Hacohen N, Brenner MB (2011). Lysosomal trafficking, antigen presentation, and microbial killing are controlled by the Arf-like GTPase Arl8b. Immunity 35, 182–193.

Graham DB *et al.* (2006). Vav1 controls DAP10-mediated natural cytotoxicity by regulating actin and microtubule dynamics. J Immunol 177, 2349–2355.

Haddad EK, Wu X, Hammer JA 3rd, Henkart PA (2001). Defective granule exocytosis in Rab27a-deficient lymphocytes from Ashen mice. J Cell Biol 152, 835–842.

Hill E, Clarke M, Barr FA (2000). The Rab6-binding kinesin, Rab6-KIFL, is required for cytokinesis. EMBO J 19, 5711–5719.

Hirokawa N (1998). Kinesin and dynein superfamily proteins and the mechanism of organelle transport. Science 279, 519–526.

Hofmann I, Munro S (2006). An N-terminally acetylated Arf-like GTPase is localised to lysosomes and affects their motility. J Cell Sci 119, 1494–1503.

Horgan CP, McCaffrey MW (2011). Rab GTPases and microtubule motors. Biochem Soc Trans 39, 1202–1206.

Hume AN, Seabra MC (2011). Melanosomes on the move: a model to understand organelle dynamics. Biochem Soc Trans 39, 1191–1196.

Hu ZZ, Valencia JC, Huang H, Chi A, Shabanowitz J, Hearing VJ, Appella E, Wu C (2007). Comparative bioinformatics analyses and profiling of lysosome-related organelle proteomes. Int J Mass Spectrom 259, 147–160.

Jordens I, Fernandez-Borja M, Marsman M, Dusseljee S, Janssen L, Calafat J, Janssen H, Wubbolts R, Neefjes J (2001). The Rab7 effector protein RILP controls lysosomal transport by inducing the recruitment of dynein-dynactin motors. Curr Biol 11, 1680–1685.

Kanwar N, Wilkins JA (2011). IQGAP1 involvement in MTOC and granule polarization in NK-cell cytotoxicity. Eur J Immunol 41, 2763–2773.

Kirkegaard T, Jaattela M (2009). Lysosomal involvement in cell death and cancer. Biochim Biophys Acta 1793, 746–754.

Kohl S, Springer TA, Schmalstieg FC, Loo LS, Anderson DC (1984). Defective natural killer cytotoxicity and polymorphonuclear leukocyte antibody-dependent cellular cytotoxicity in patients with LFA-1/OKM-1 deficiency. J Immunol 133, 2972–2978.

Korolchuk VI *et al.* (2011). Lysosomal positioning coordinates cellular nutrient responses. Nat Cell Biol 13, 453–460.

Kurowska M, Goudin N, Nehme NT, Court M, Garin J, Fischer A, de Saint Basile G, Menasche G (2012). Terminal transport of lytic granules to the immune synapse is mediated by the kinesin-1/Slp3/Rab27a complex. Blood 119, 3879–3889.

Liu D, Meckel T, Long EO (2010). Distinct role of rab27a in granule movement at the plasma membrane and in the cytosol of NK cells. PLoS One 5, e12870.

Lowin-Kropf B, Shapiro VS, Weiss A (1998). Cytoskeletal polarization of T cells is regulated by an immunoreceptor tyrosine-based activation motif-dependent mechanism. J Cell Biol 140, 861–871.

Matesic LE, Yip R, Reuss AE, Swing DA, O'Sullivan TN, Fletcher CF, Copeland NG, Jenkins NA (2001). Mutations in Mlph, encoding a member of the Rab effector family, cause the melanosome transport defects observed in leaden mice. Proc Natl Acad Sci USA 98, 10238–10243.

Menasche G *et al.* (2000). Mutations in RAB27A cause Griscelli syndrome associated with haemophagocytic syndrome. Nat Genet 25, 173–176.

Mentlik AN, Sanborn KB, Holzbaur EL, Orange JS (2010). Rapid lytic granule convergence to the MTOC in natural killer cells is dependent on dynein but not cytolytic commitment. Mol Biol Cell 21, 2241–2256.

Mercer JA, Seperack PK, Strobel MC, Copeland NG, Jenkins NA (1991). Novel myosin heavy chain encoded by murine dilute coat colour locus. Nature 349, 709–713.

Mohamed MM, Sloane BF (2006). Cysteine cathepsins: multifunctional enzymes in cancer. Nat Rev Cancer 6, 764–775.

Okai T, Araki Y, Tada M, Tateno T, Kontani K, Katada T (2004). Novel small GTPase subfamily capable of associating with tubulin is required for chromosome segregation. J Cell Sci 117, 4705–4715.

Orange JS (2008). Formation and function of the lytic NK-cell immunological synapse. Nat Rev Immunol 8, 713–725.

Orange JS, Harris KE, Andzelm MM, Valter MM, Geha RS, Strominger JL (2003). The mature activating natural killer cell immunologic synapse is formed in distinct stages. Proc Natl Acad Sci USA 100, 14151–14156.

Raposo G, Marks MS (2007). Melanosomes—dark organelles enlighten endosomal membrane transport. Nat Rev Mol Cell Biol 8, 786–797.

Rosa-Ferreira C, Munro S (2011). Arl8 and SKIP act together to link lysosomes to kinesin-1. Dev Cell 21, 1171–1178.

Sanchez-Ruiz J, Mejias R, Garcia-Belando M, Barber DF, Gonzalez-Garcia A (2011). Ral GTPases regulate cell-mediated cytotoxicity in NK cells. J Immunol 187, 2433–2441.

Sancho D, Nieto M, Llano M, Rodriguez-Fernandez JL, Tejedor R, Avraham S, Cabanas C, Lopez-Botet M, Sanchez-Madrid F (2000). The tyrosine kinase PYK-2/RAFTK regulates natural killer (NK) cell cytotoxic response, and is translocated and activated upon specific target cell recognition and killing. J Cell Biol 149, 1249–1262.

Stinchcombe JC, Barral DC, Mules EH, Booth S, Hume AN, Machesky LM, Seabra MC, Griffiths GM (2001). Rab27a is required for regulated secretion in cytotoxic T lymphocytes. J Cell Biol 152, 825–834.

Stinchcombe JC, Griffiths GM (2007). Secretory mechanisms in cell-mediated cytotoxicity. Annu Rev Cell Dev Biol 23, 495–517.

Stinchcombe JC, Majorovits E, Bossi G, Fuller S, Griffiths GM (2006). Centrosome polarization delivers secretory granules to the immunological synapse. Nature 443, 462–465.

Stinchcombe JC, Salio M, Cerundolo V, Pende D, Arico M, Griffiths GM (2011). Centriole polarisation to the immunological synapse directs secretion from cytolytic cells of both the innate and adaptive immune systems. BMC Biol 9, 45.

Stowers L, Yelon D, Berg LJ, Chant J (1995). Regulation of the polarization of T cells toward antigen-presenting cells by Ras-related GTPase CDC42. Proc Natl Acad Sci USA 92, 5027–5031.

Strom M, Hume AN, Tarafder AK, Barkagianni E, Seabra MC (2002). A family of Rab27-binding proteins. Melanophilin links Rab27a and myosin Va function in melanosome transport. J Biol Chem 277, 25423–25430.

Tanaka Y, Kanai Y, Okada Y, Nonaka S, Takeda S, Harada A, Hirokawa N (1998). Targeted disruption of mouse conventional kinesin heavy chain, kif5B, results in abnormal perinuclear clustering of mitochondria. Cell 93, 1147–1158.

Ueno H, Huang X, Tanaka Y, Hirokawa N (2011). KIF16B/Rab14 molecular motor complex is critical for early embryonic development by transporting FGF receptor. Dev Cell 20, 60–71.

Vale RD, Fletterick RJ (1997). The design plan of kinesin motors. Annu Rev Cell Dev Biol 13, 745–777.

Wagtmann N, Rajagopalan S, Winter CC, Peruzzi M, Long EO (1995). Killer cell inhibitory receptors specific for HLA-C and HLA-B identified by direct binding and by functional transfer. Immunity 3, 801–809.

Wu X, Wang F, Rao K, Sellers JR, Hammer JA 3rd (2002). Rab27a is an essential component of melanosome receptor for myosin Va. Mol Biol Cell 13, 1735–1749.

Yodoi J *et al.* (1985). TCGF (IL 2)-receptor inducing factor(s). I. Regulation of IL 2 receptor on a natural killer-like cell line (YT cells). J Immunol 134, 1623–1630.

Supplemental Materials

Molecular Biology of the Cell

Tuli et al.

Supplementary Figures

Figure S1: Arl8b co-localizes with perforin in YT-Indy cells. Serial *z*-sections were obtained every 0.2 μm, and the crosshairs depict common membrane structures on a representative micrograph containing both Arl8b (green) and Pfn (red). Nucleus was stained with DAPI (blue). Scale bar 10 μm.

Figure S2: Silencing of Arl8b and Rab27a in NK cells. A) Primary NK cells were electroporated with control- or Arl8b- siRNA. After 72 hr, a qRT-PCR analysis was performed using Arl8b and Arl8a specific primers. **B)** Silencing of Rab27a in YT-Indy cells. Stable silencing of Rab27a was achieved in YT-Indy cells by introducing lentiviral vector-driven shRNA against Rab27a and qRT-PCR was performed to check the efficiency of Rab27a silencing.

Figure S3: Arl8a silencing inhibits NK cytotoxicity but to a lesser extent compared to Arl8b. A) qRT-PCR analyses of Arl8b and Arl8a levels in control shRNA-, Arl8a 497 shRNA-, and Arl8a 1685 shRNA-expressing YT-Indy cells. **B)** YT-Indy cells stably expressing control shRNA, Arl8b-specific shRNA (407 and 921) or Arl8a-specific shRNA (497 and 1685) were tested against 721.221 target cells by ^{51}Cr-release assay at various E:T cell ratios. Data show mean ± SEM of triplicates from one representative experiment of three performed.

Figure S4: Arl8b silencing does not prevent F-actin polarization, and Arl8a and Rab27a silencing does not affect lytic granule polarization in NK cells. A) YT-Indy cells stably transduced with control shRNA (left panel) or Arl8b shRNA (right panel) were mixed with anti-LFA1 mAb-coated polystyrene beads for 60 min at 37°C. The cells were then stained with AlexaFluor 488-conjugated phalloidin (green) to visualize F-actin. **B)** The percentage of lytic granule (marked by perforin staining) polarization in control- versus Arl8a-silenced-YT-Indy

cells. Bar graph represents mean ± SD of three independent experiments; at least 50 conjugates were evaluated in each experiment. No significant difference was observed between the groups. **C)** Confocal analyses was performed on YT-Indy cells stably transduced with control shRNA (left panel) or Rab27a-specific shRNA (right panel) and mixed with 721.221 target cells for 20 min at the E:T ratio of 2:1. Conjugates were fixed and stained using anti-perforin antibody (green) and the MTOC was marked by anti-pericentrin antibody staining (red). Scale bar, 10 μm.

Figure S5: Dynein activity is required for perinuclear clustering of lysosomes observed upon Arl8b silencing. A) HeLa cells were treated with control siRNA (left panel), Arl8b siRNA (middle panel) or Arl8b siRNA plus dynein siRNA (right panel) for 72 hr. Following siRNA treatment, cells were fixed and stained with anti-LAMP-1 antibody to visualize lysosomes by confocal microscopy. **B-C)** HeLa treated with control siRNA (B) or Arl8b siRNA (C). Post 48 hr siRNA treatment, cells were transfected with CC1-GFP (green) to inhibit dynein activity. Post 24 hr transfection, cells were fixed and stained with anti-LAMP-1 antibody (red) to visualize lysosomes by confocal microscopy.

Figure S6: List of proteins identified as Arl8b binding partners from NK cell lysates. GST-pull down assay was performed using YT-Indy cell lysates with GST-Arl8b or GST alone. Eluates were run on SDS-PAGE. Bands which appeared specifically in the GST-Arl8b lane were excised, partially digested with trypsin, and analyzed by mass spectrometry. The number of unique peptides identified corresponding to each interaction partner is listed at right. Four unique peptides corresponding to KIF5B motor protein were identified using this approach (highlighted in bold).

Figure S7: Silencing of Kif5B in HeLa and NK cells. A-D) Silencing of Arl8b or Kif5b causes perinuclear clustering of lysosomes. HeLa cells were treated with control siRNA (A), Arl8b siRNA (B) or Kif5B siRNA (C). Following 72 hrs treatment, cells were fixed, stained with anti-LAMP-1 antibody and analyzed by confocal microscopy. The silencing efficiency of Kif5B was assessed by Western blot (D). Actin blot was performed to show equal protein loading. **E)** Stable silencing of Kif5B expression was achieved in YT-Indy cells by introducing lentiviral vector-driven shRNA against Kif5B. Western blot was performed to check the efficiency of Kif5B silencing and β-actin blot was done as a control to show equal protein loading.

Figure S1

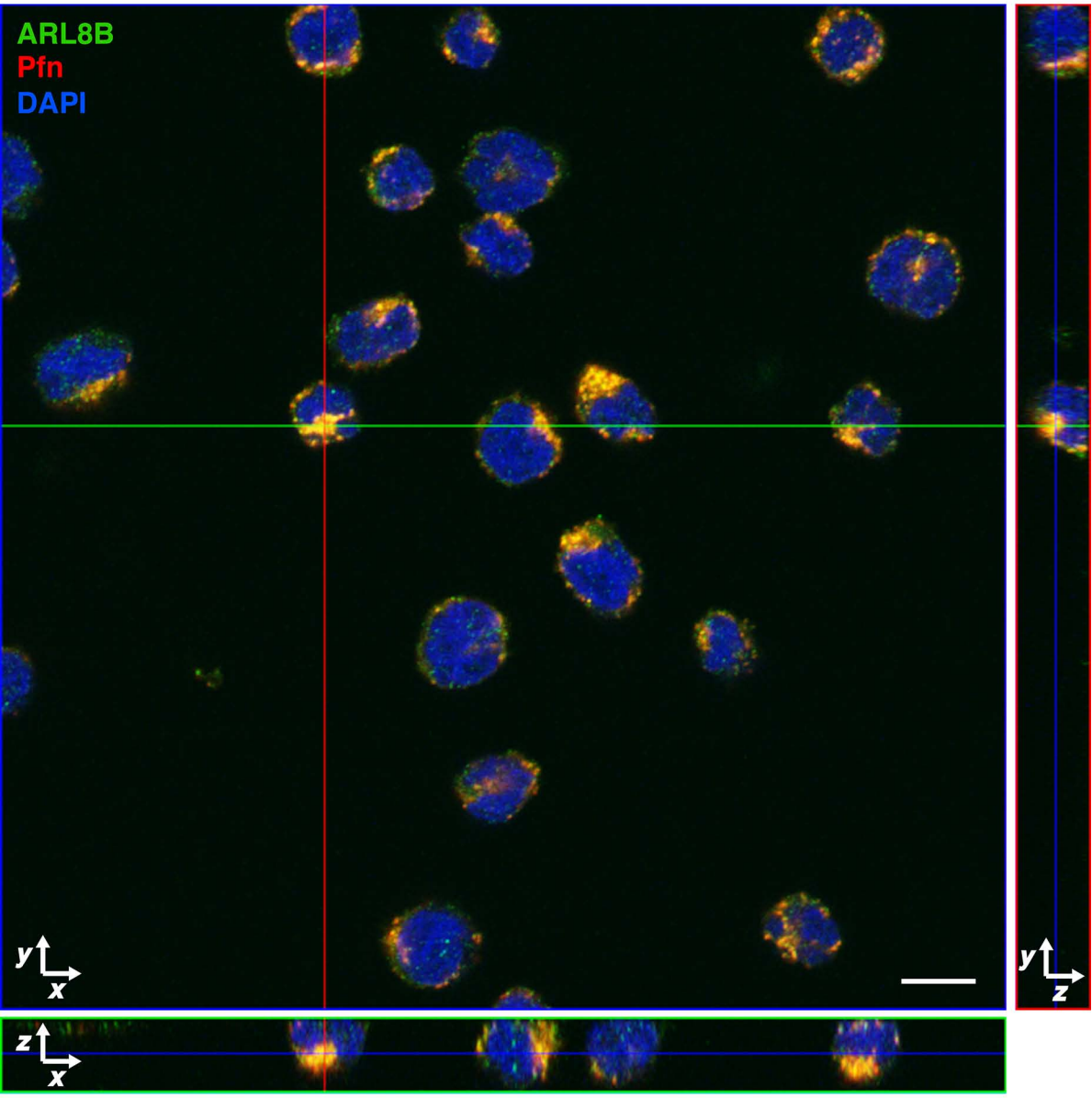

Figure S2

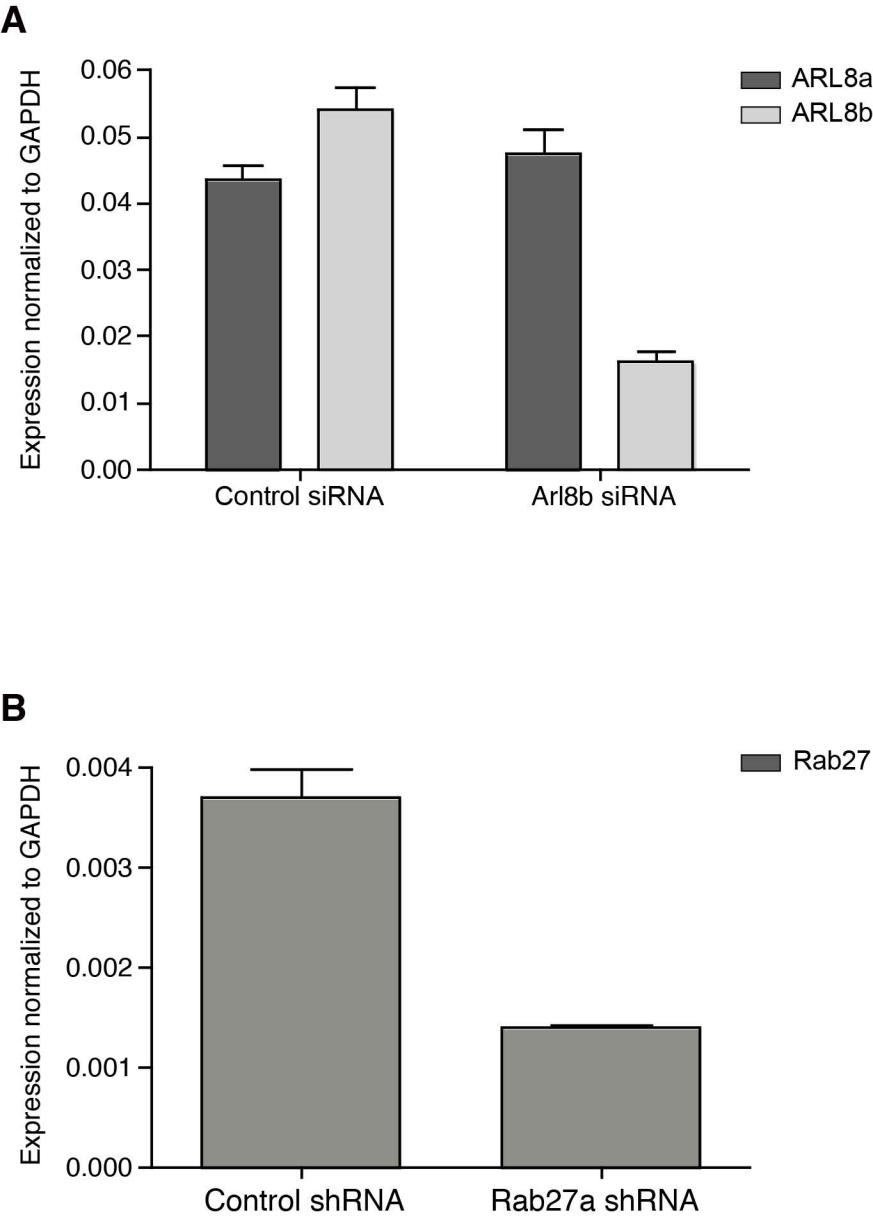
A
0.06
0.05
0.04
0.03
0.02
0.01
0.00
Expression normalized to GAPDH
ARL8a
ARL8b
Control siRNA
Arl8b siRNA
B
0.004
0.003
0.002
0.001
0.000
Expression normalized to GAPDH
Rab27
Control shRNA
Rab27a shRNA

Figure S3

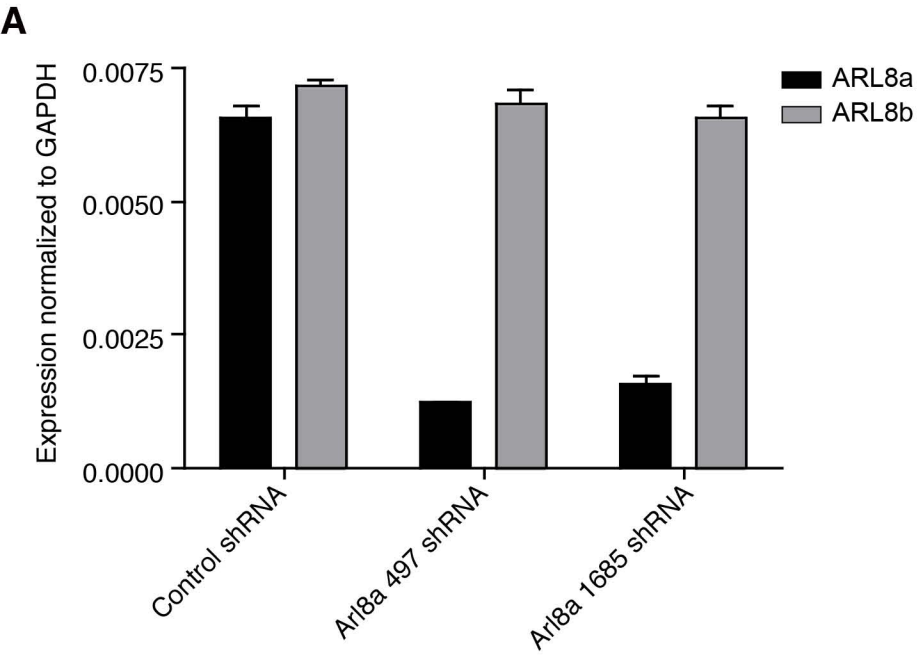
A
Expression normalized to GAPDH
0.0075
0.0050
0.0025
0.0000
ARL8a
ARL8b
Control shRNA
Arl8a 497 shRNA
Arl8a 1685 shRNA

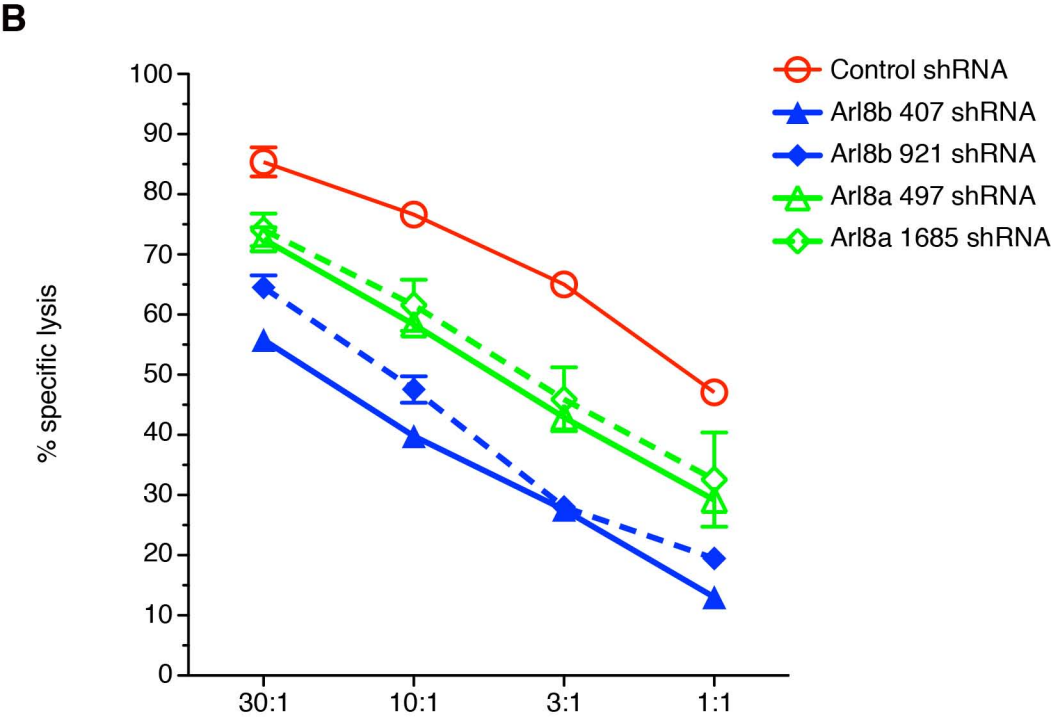
B
% specific lysis
100
90
80
70
60
50
40
30
20
10
0
30:1
10:1
3:1
1:1
Control shRNA
Arl8b 407 shRNA
Arl8b 921 shRNA
Arl8a 497 shRNA
Arl8a 1685 shRNA

Figure S4

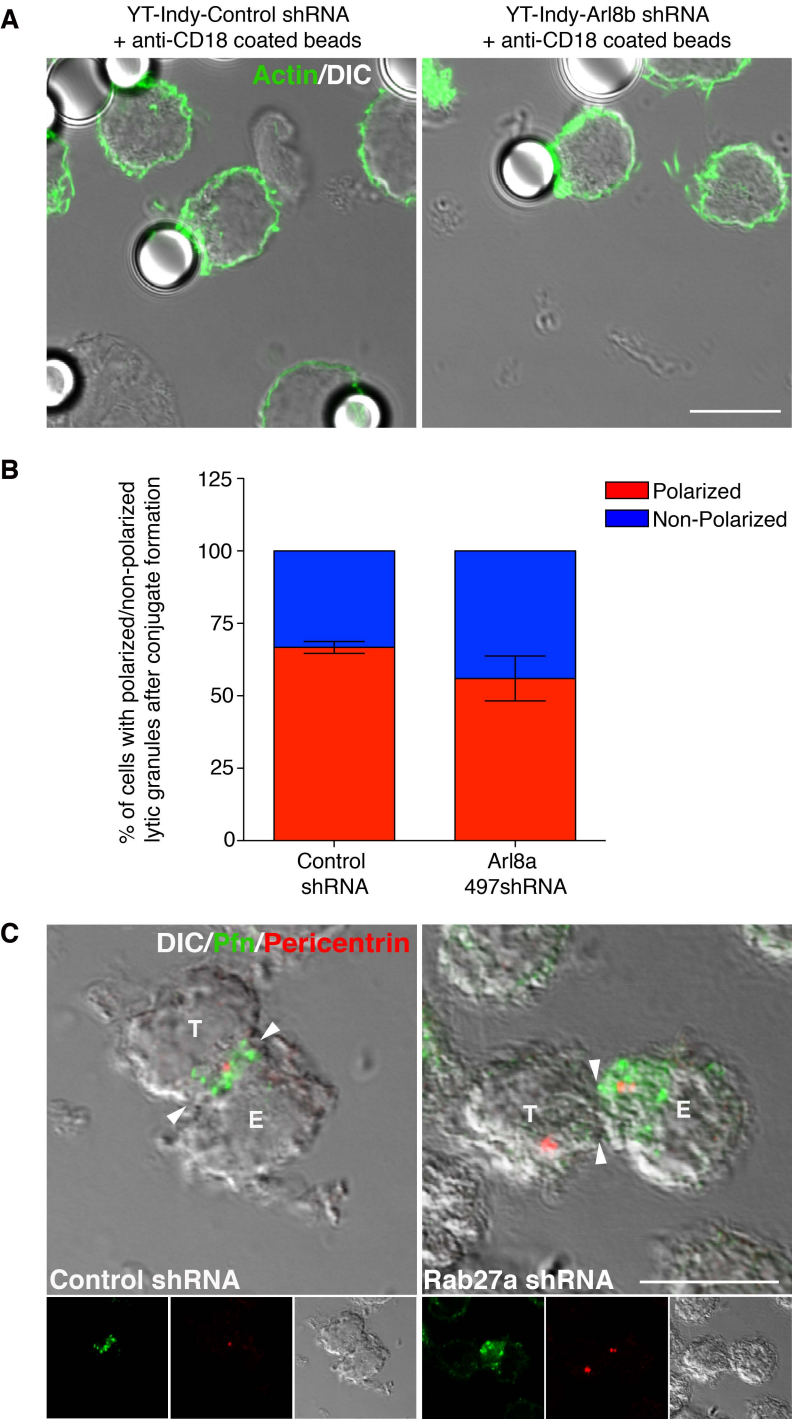
A
YT-Indy-Control shRNA
+ anti-CD18 coated beads
YT-Indy-Arl8b shRNA
+ anti-CD18 coated beads
Actin/DIC
B
% of cells with polarized/non-polarized
lytic granules after conjugate formation
125
100
75
50
25
0
Polarized
Non-Polarized
Control
shRNA
Arl8a
497shRNA
C
DIC/Pfn/Pericentrin
T
E
Control shRNA
T
E
Rab27a shRNA

Figure S5

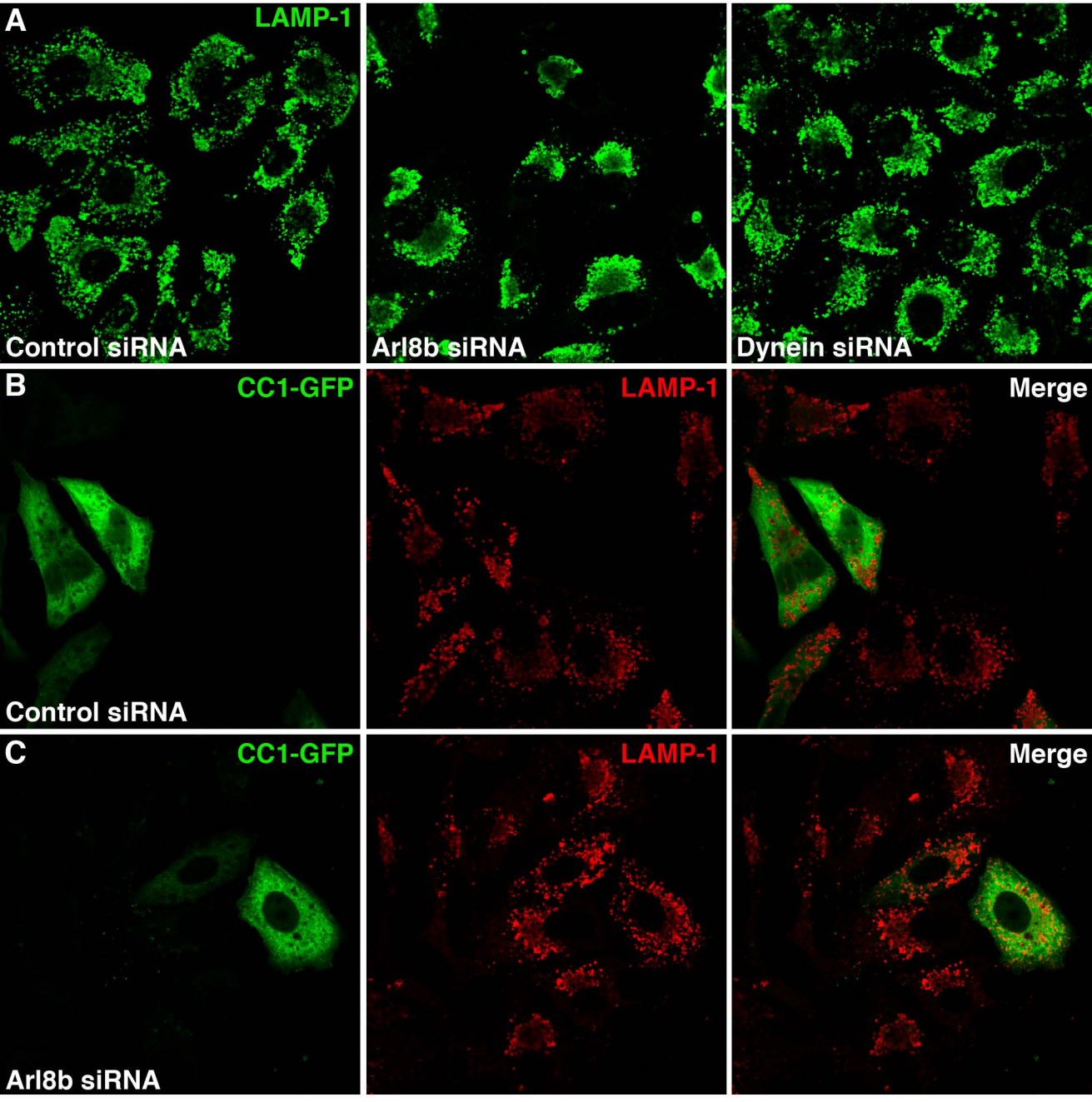
A
LAMP-1
Control siRNA
Arl8b siRNA
Dynein siRNA
B
CC1-GFP
LAMP-1
Merge
Control siRNA
C
CC1-GFP
LAMP-1
Merge
Arl8b siRNA

Figure S6

Arl8b-interacting proteins	# of unique peptides
TUBB2C Tubulin beta-2C chain	30
TUBA4A Tubulin alpha-4A chain	28
TUBB3 Tubulin beta-3 chain	11
TBCD Isoform 4 of Tubulin-specific chaperone D	9
CCT2 T-complex protein 1 subunit beta	9
ATP6V1A V-type proton ATPase catalytic subunit A	7
KANK2 KN motif and ankyrin repeat domains 2	4
KIF5B Kinesin-1 heavy chain	**4**
FAF2 FAS-associated factor 2	3
LMNA Isoform A of Lamin-A/C	3
IFI16 Isoform 1 of Gamma-interferon-inducible protein Ifi-16	3
VIM Vimentin	3
Vps16 Isoform 1 of Vacuolar protein sorting-associated protein 16 homolog	2
Vps18 of Vacuolar protein sorting-associated protein 18 homolog	2
ANXA2P2 Putative annexin A2-like protein	2

Figure S7

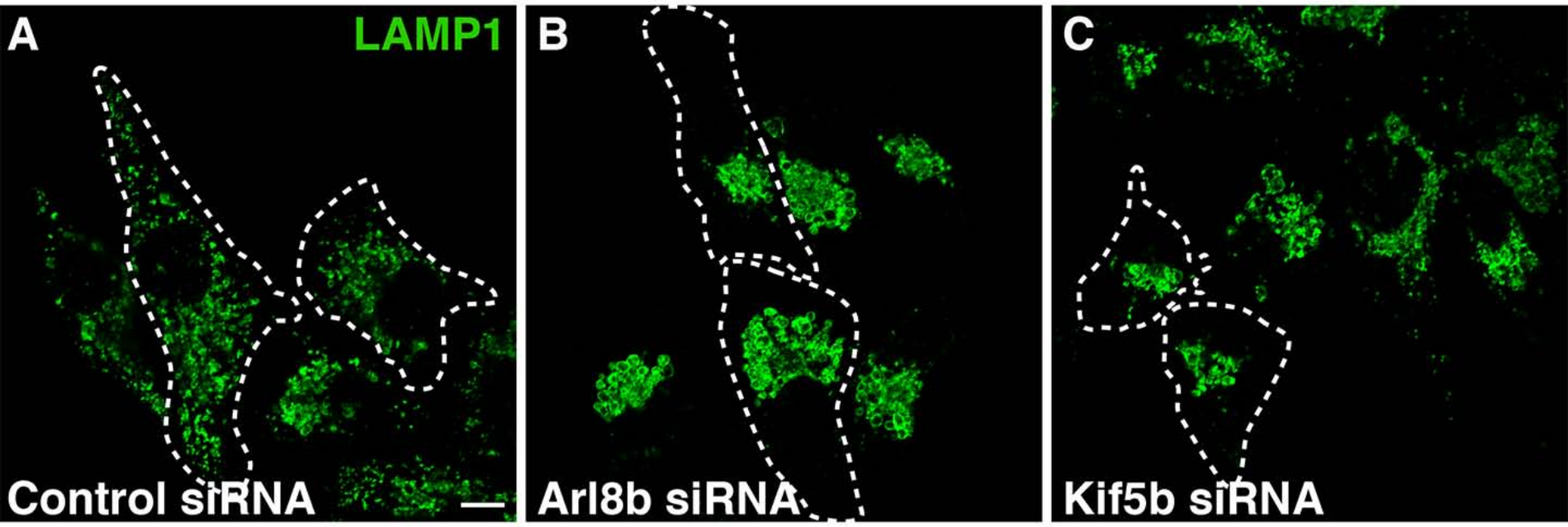
A
LAMP1
Control siRNA
B
Arl8b siRNA
C
Kif5b siRNA

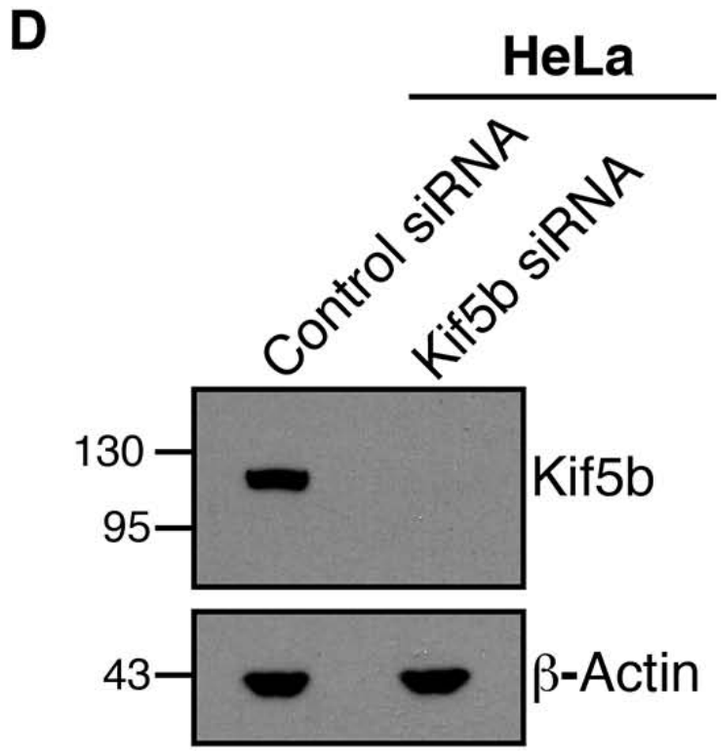
D
HeLa
Control siRNA
Kif5b siRNA
130
95
Kif5b
43
β-Actin

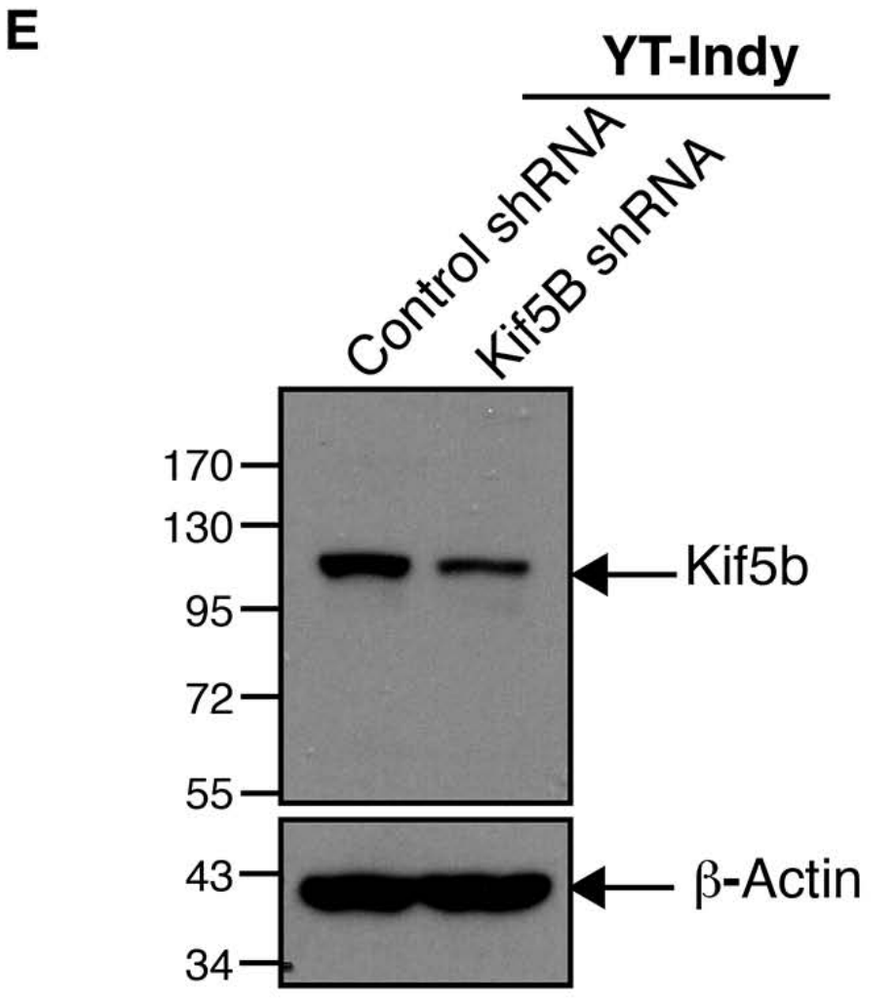
E
YT-Indy
Control shRNA
Kif5B shRNA
170
130
95
72
55
Kif5b
43
34
β-Actin